# SELF-ADAPTIVE *hp* FINITE-ELEMENT SIMULATION OF MULTI-COMPONENT INDUCTION MEASUREMENTS ACQUIRED IN DIPPING, INVADED, AND ANISOTROPIC FORMATIONS

**M. J. Nam[1], D. Pardo[2*], and C. Torres-Verdín[1],**

[1]The University of Texas at Austin, USA
[2]Basque Center for Applied Mathematics, Spain
[*]Formerly, at The University of Texas at Austin, USA

Presentation at SIG meeting (SPWLA) Oct. 21, 2008.

Houston, TX, USA

THE UNIVERSITY OF TEXAS AT AUSTIN

# Outline

- **Main Features of Our Technology**
  - A Self-Adaptive Goal-Oriented *hp*-FEM
  - Fourier Finite-Element Method
- **Introduction to Tri-Axial Induction**
- **Numerical Results:**
  - in Dipping, Invaded, Anisotropic Formations (Resistive Mandrel )
  - with Tool Eccentricity (Conductive / Resistive Mandrel)
- **Conclusions**

# Self-Adaptive Goal-Oriented *hp*-FEM

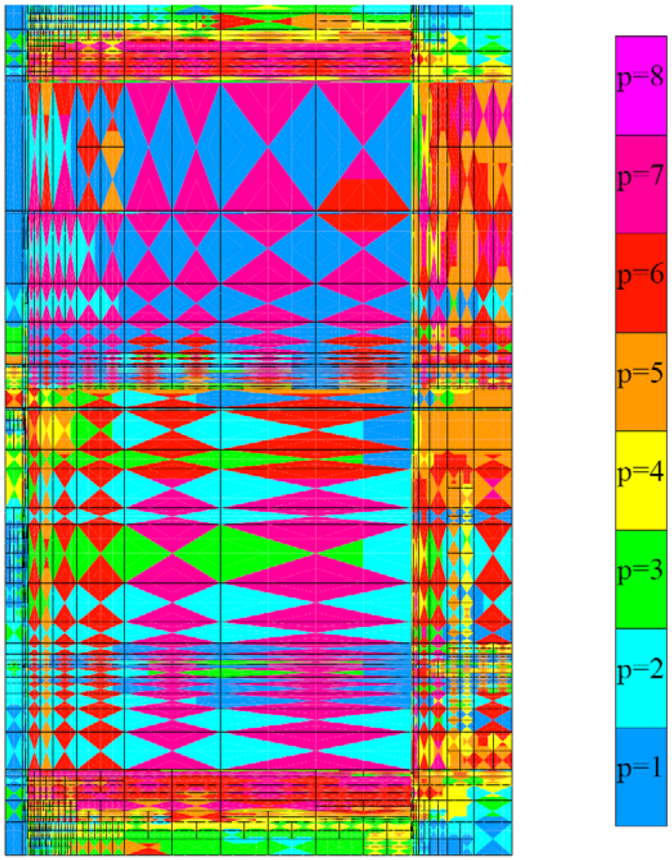


We vary locally the element size ***h*** and the polynomial order of approximation ***p*** throughout the grid.

Optimal grids are **automatically generated** by the *hp*-algorithm.

The self-adaptive goal-oriented *hp*-FEM provides **exponential convergence** rates in terms of the CPU time vs. the error in a **user prescribed quantity of Interest**.

# 3D Deviated Well

**Cartesian system of coordinates:** $(x_1, x_2, x_3)$

**New non-orthogonal system of coordinates:** $(\zeta_1, \zeta_2, \zeta_3)$

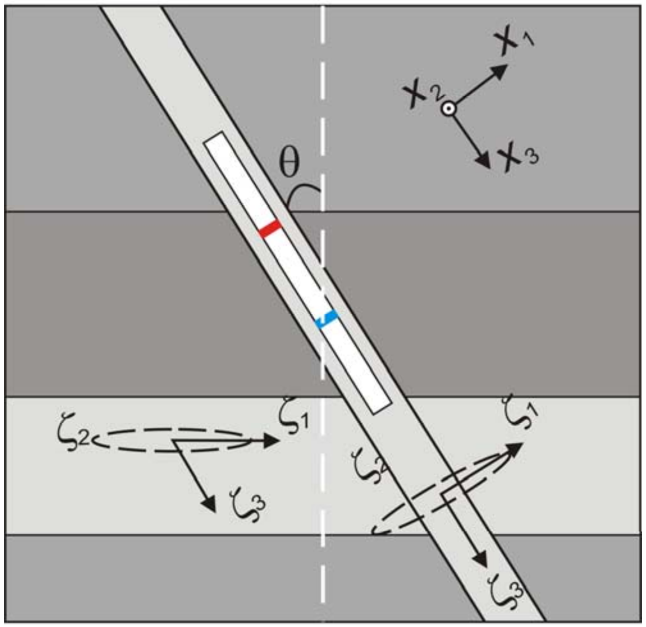


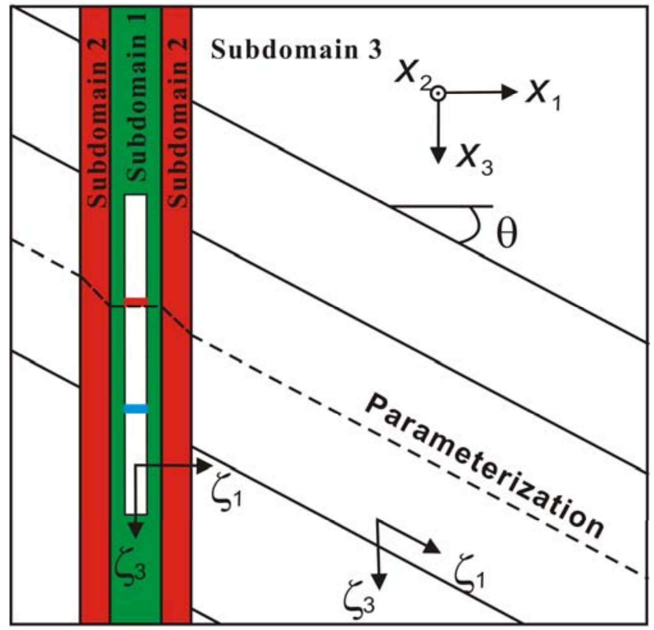


**Subdomain 1**

$$\begin{cases} x_1 = \zeta_1 \cos \zeta_2 \\ x_2 = \zeta_1 \sin \zeta_2 \\ x_3 = \zeta_3 \end{cases}$$

**Subdomain 2**

$$\begin{cases} x_1 = \zeta_1 \cos \zeta_2 \\ x_2 = \zeta_1 \sin \zeta_2 \\ x_3 = \zeta_3 + \tan\theta \dfrac{\zeta_1 - \rho_1}{\rho_2 - \rho_1} \rho_2 \cos \zeta_2 \end{cases}$$

**Subdomain 3**

$$\begin{cases} x_1 = \zeta_1 \cos \zeta_2 \\ x_2 = \zeta_1 \sin \zeta_2 \\ x_3 = \zeta_3 + \zeta_1 \tan\theta \cos \zeta_2 \end{cases}$$

# 3D Deviated Well

**Cartesian system of coordinates:** $(x_1, x_2, x_3)$

**New non-orthogonal system of coordinates:** $(\zeta_1, \zeta_2, \zeta_3)$

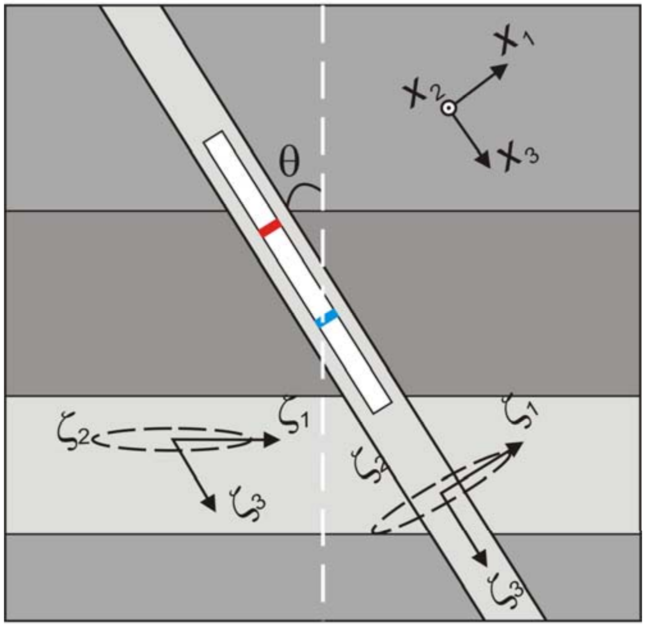


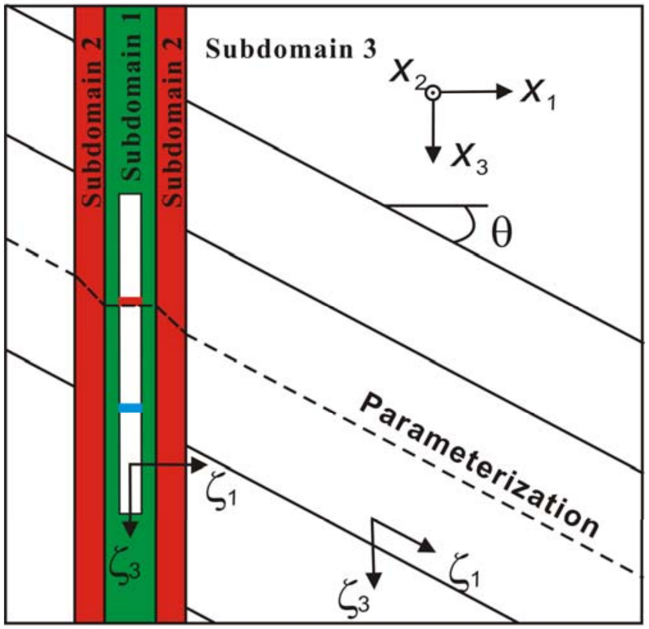


**Constant material coefficients in the quasi-azimuthal direction $\zeta_2$ in the new non-orthogonal system of coordinates!!!!**

# Fourier Series Expansion in $\zeta_2$

**Fourier Series Expansion of a Function $\omega$ in $\zeta_2$:**

$$\omega = \sum_{l=-\infty}^{l=\infty} \omega_l e^{jl\zeta_2} = \sum_{l=-\infty}^{l=\infty} F_l(\omega) e^{jl\zeta_2}$$

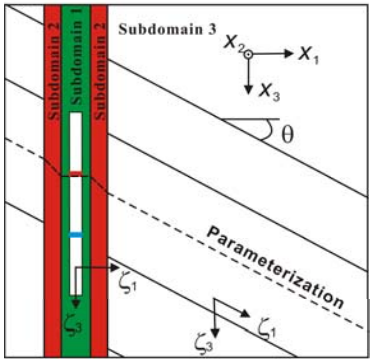


**Final Variational Formulation of DC after Fourier Series Expansion in $\zeta_2$:**

$$\begin{cases} \text{Find } F_l(u) \in F_l(\underline{u}_D) + H_D^1(\Omega_{2D}) \text{ such that:} \\ \displaystyle\sum_{k=-\infty}^{k=\infty} \sum_{l=k-2}^{l=k+2} < F_k\left(\frac{\partial v}{\partial \zeta}\right), F_{k-l}(\sigma_{NEW}) F_l\left(\frac{\partial u}{\partial \zeta}\right) >_{L^2(\Omega_{2D})} \\ \displaystyle = \sum_{k=-\infty}^{k=\infty} \left[ < F_k(v), F_k(f_{NEW}) >_{L^2(\Omega_{2D})} + < F_k(v), F_k(g_{NEW}) >_{L^2(\Omega_{2D})} \right] \quad \forall F_k(v) \in H_D^1(\Omega), \end{cases}$$

**← Mono-modal test function:**

$$v = v_k e^{jk\zeta_2}$$

**because** $F_{k-l}(\sigma_{NEW}) = 0$ **for every** $|k-l| > 2$.

**Only Five Fourier Modes ( $l$ ) are enough to represent $\sigma_{NEW}$ EXACTLY for each $k$.**

**Therefore, we need to truncate only Fourier Modes ( $k$ ) for 3D solution.**

# Eccentered Tool

**Cartesian system of coordinates:** $(x_1, x_2, x_3)$

**New non-orthogonal system of coordinates:** $(\zeta_1, \zeta_2, \zeta_3)$

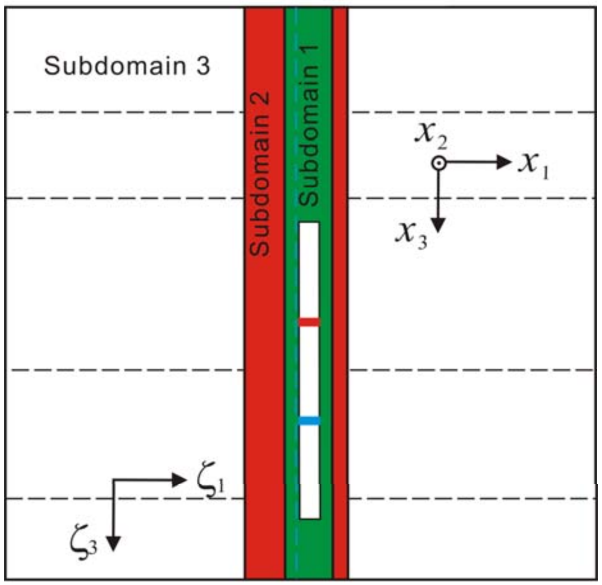


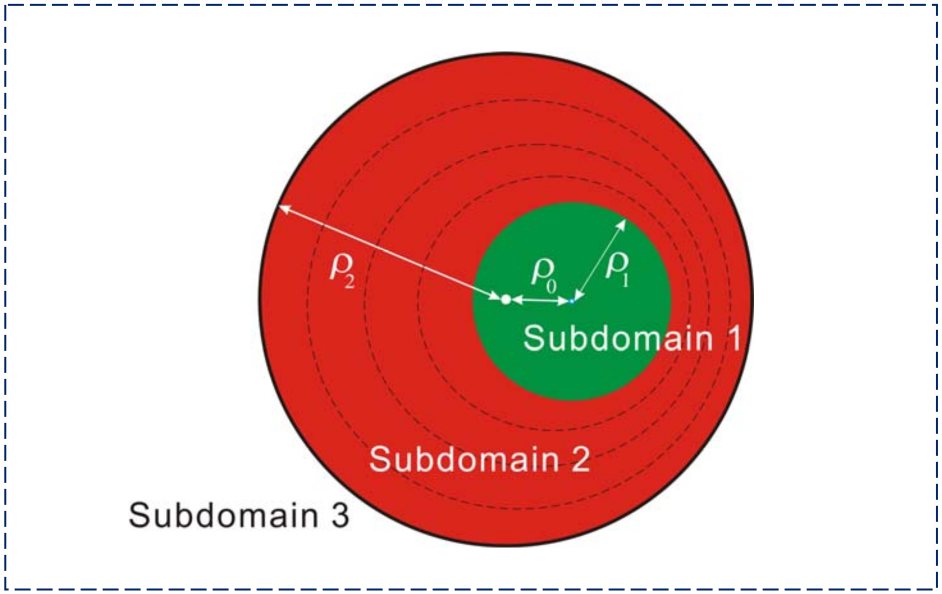


**Subdomain 1**

$$\begin{cases} x_1 = \rho_0 + \zeta_1 \cos \zeta_2 \\ x_2 = \zeta_1 \sin \zeta_2 \\ x_3 = \zeta_3 \end{cases}$$

**Subdomain 2**

$$\begin{cases} x_1 = \dfrac{\zeta_1 - \rho_2}{\rho_1 - \rho_2} \rho_0 + \zeta_1 \cos \zeta_2 \\ x_2 = \zeta_1 \sin \zeta_2 \\ x_3 = \zeta_3 \end{cases}$$

**Subdomain 3**

$$\begin{cases} x_1 = \zeta_1 \cos \zeta_2 \\ x_2 = \zeta_1 \sin \zeta_2 \\ x_3 = \zeta_3 \end{cases}$$

# Tri-Axial Induction Tool

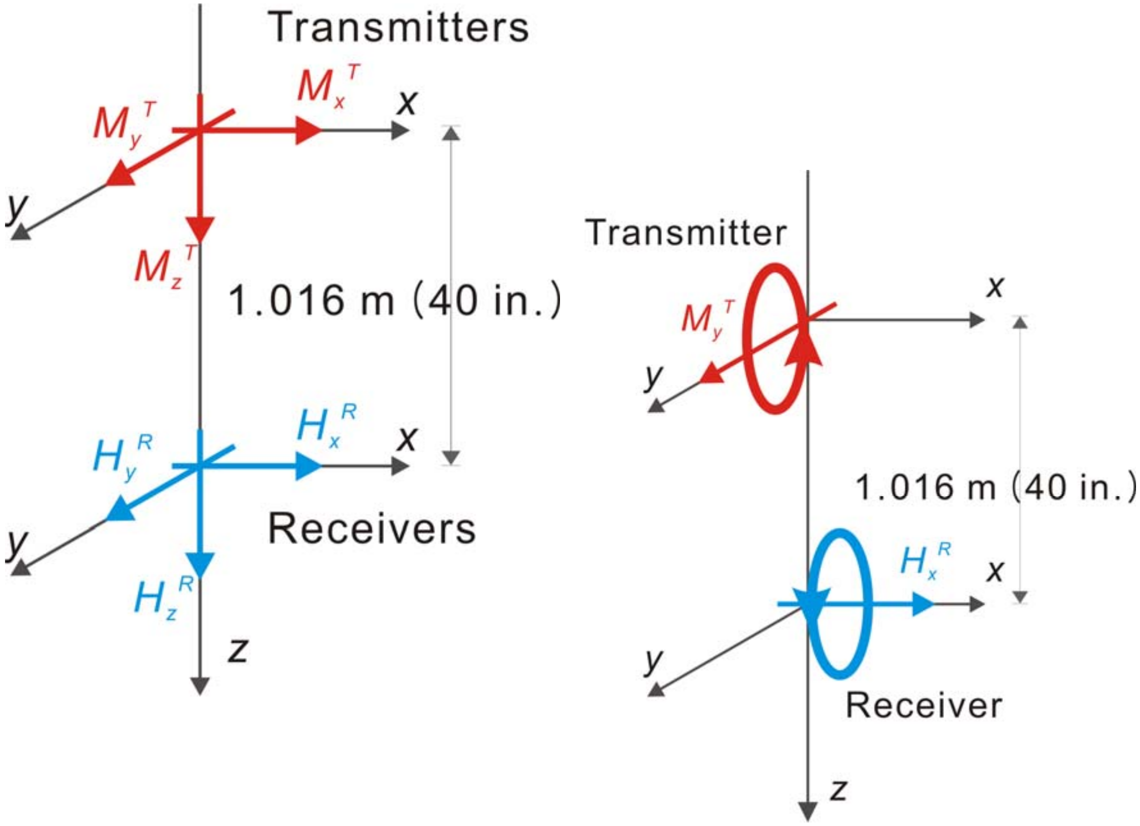


$H_{xy}$

***L = 1.016 m (40 In.)***

***Operating frequency: 20 kHz***

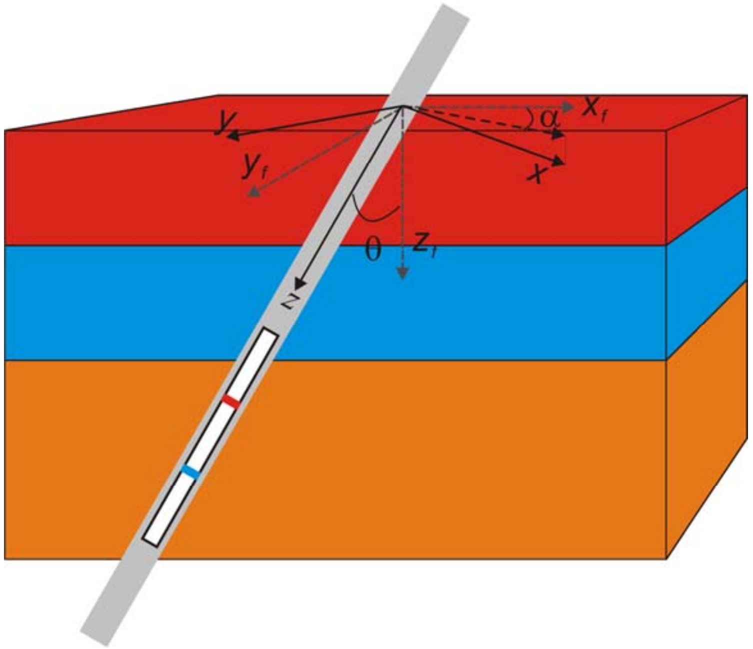


***θ: dip angle***

***α: tool orientation angle***

# 3D Source Implementation

## 1. Solenoidal Coil ($J_\phi$) for $M_z$

→ *becoming a 2D source in ($\rho$, $\phi$, z)*

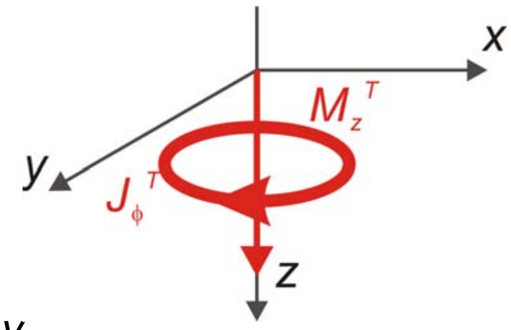


## 2. Delta Function for 3D source $M_x$ or $M_y$

$$f(\phi) = \delta(\phi - \phi_0)$$

***$\phi_0$: the position of the center of the peak (0° for $M_x$; 90° for $M_y$)***

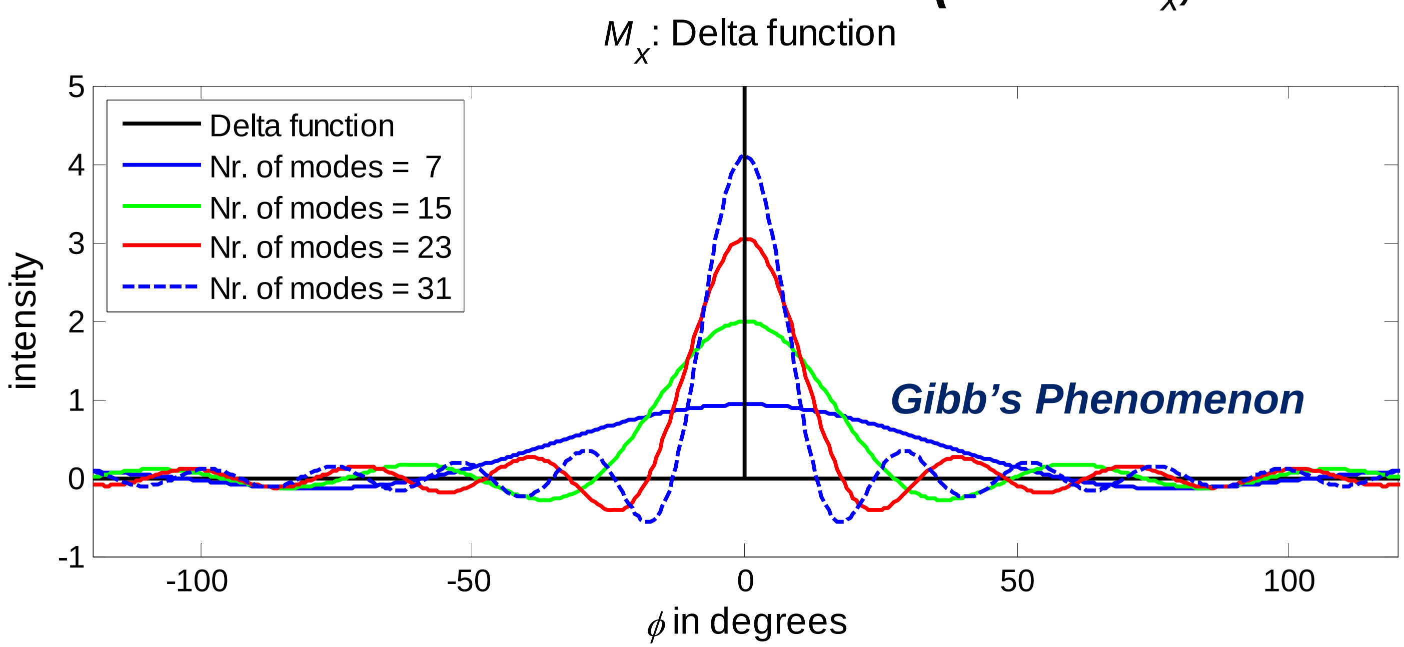


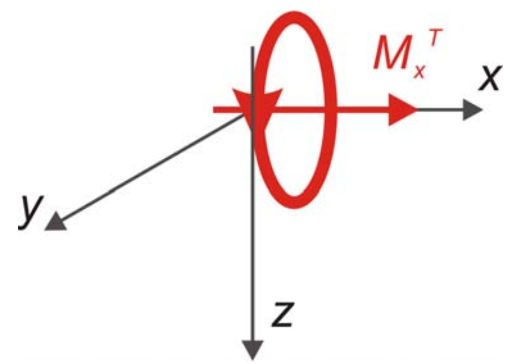

# 3D Source and Receiver (Delta Functions)

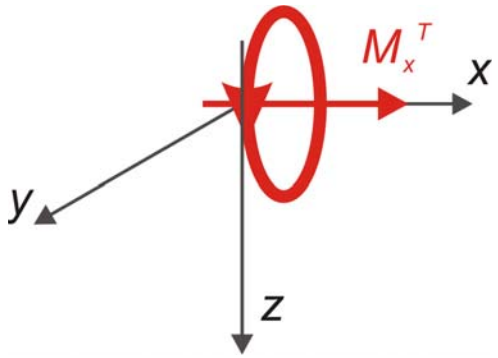


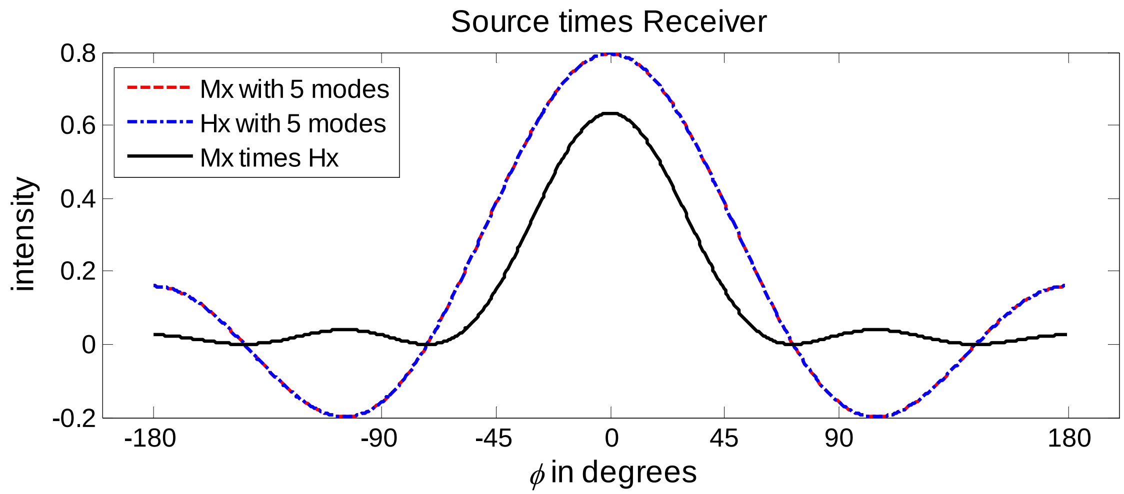


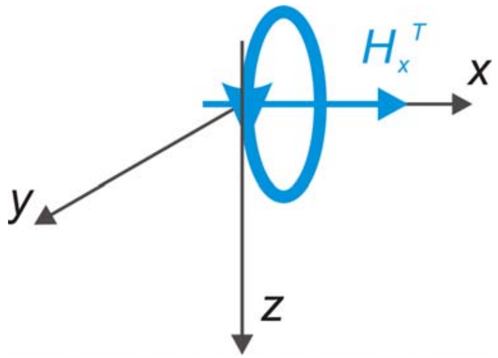


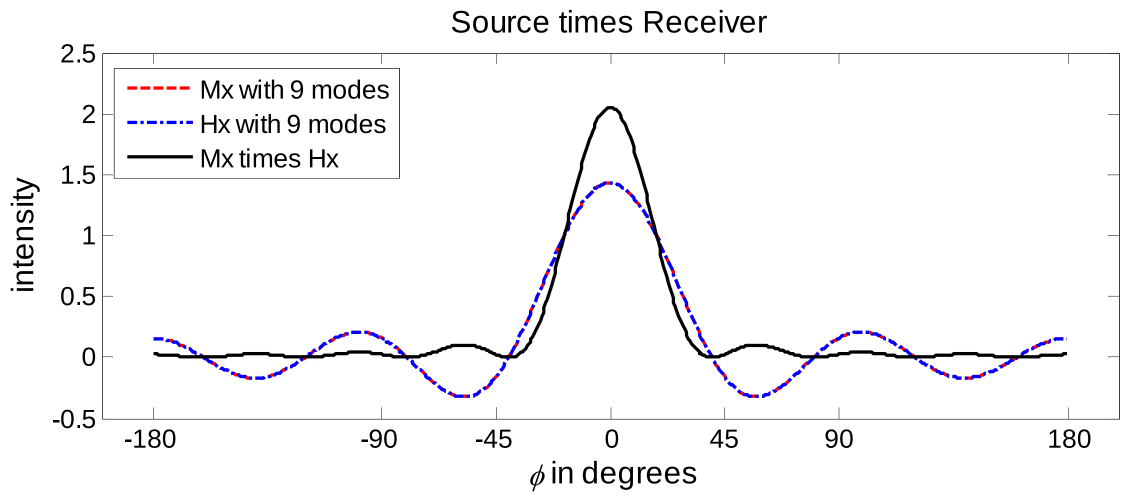


***Coupling between source and receiver: less Gibb's phenomenon***

# Verification of 2.5D Simulation ($H_{xx} = H_{yy}$)

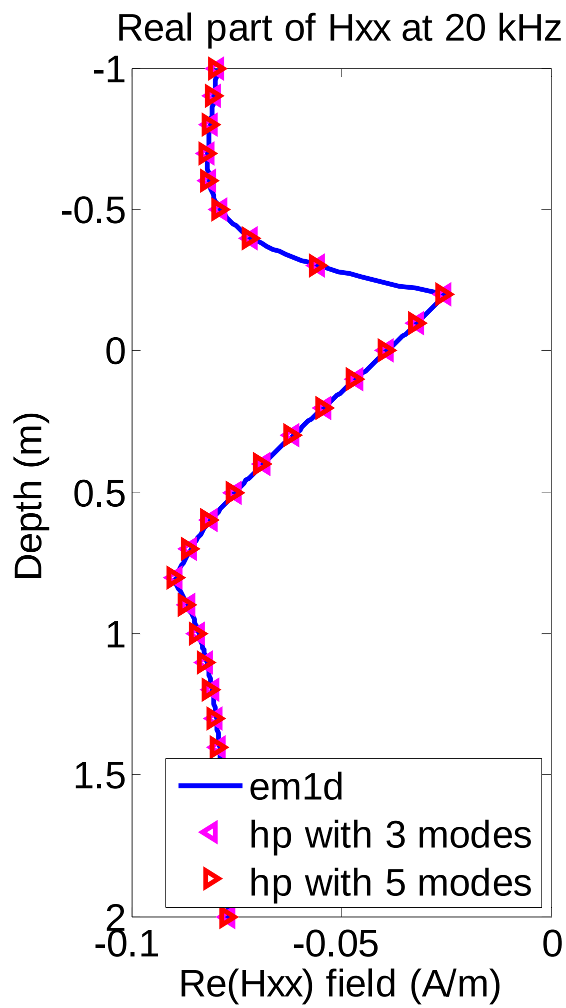


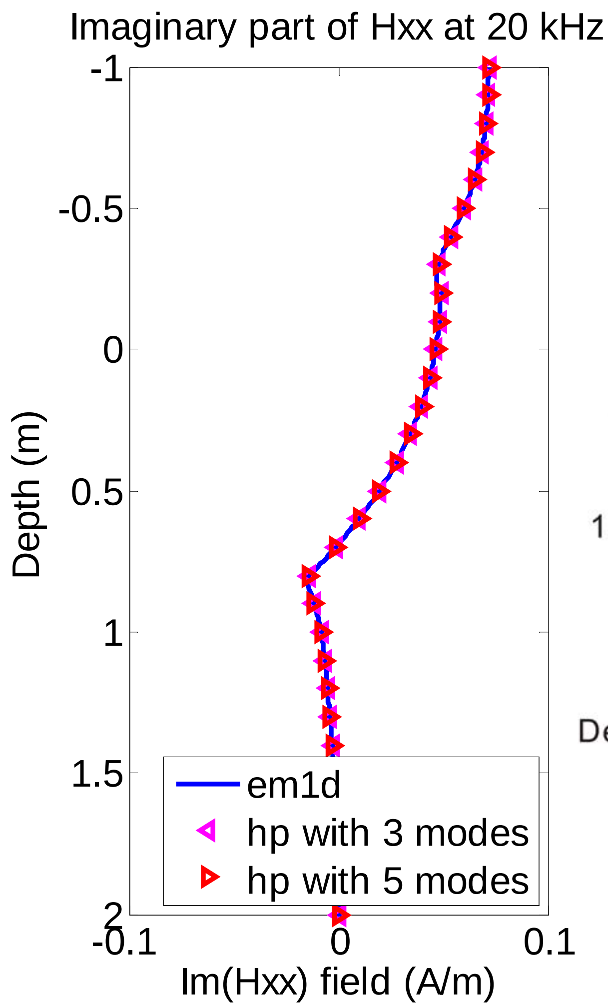


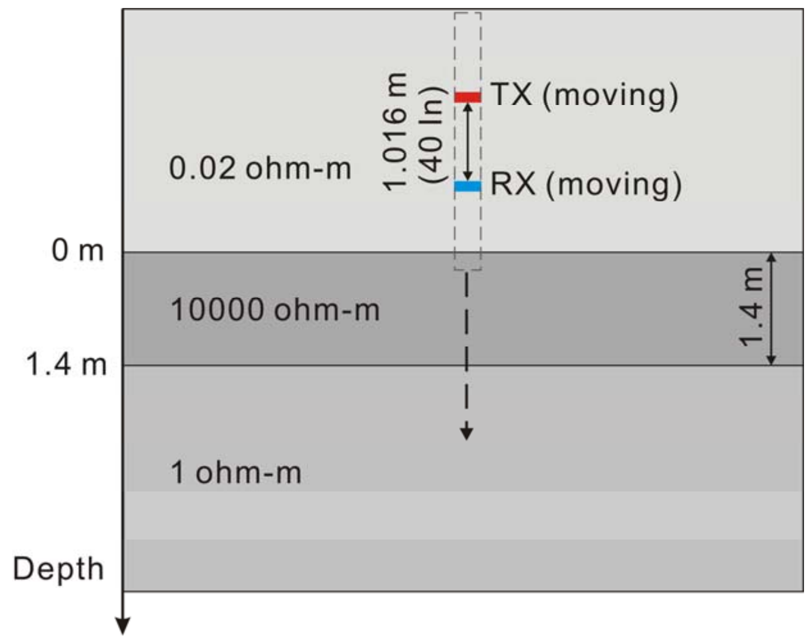


**Converged solutions with 3 Fourier modes**

em1D: K. H. Lee 1984, pers. comm.

# Verification of 2.5D Simulation ($H_{xy} = H_{yx}$)

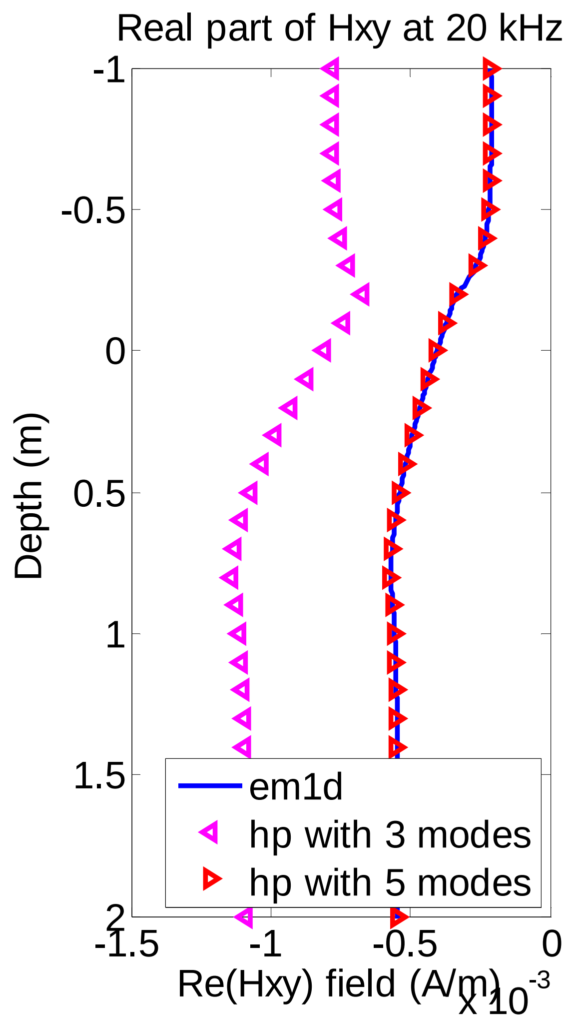


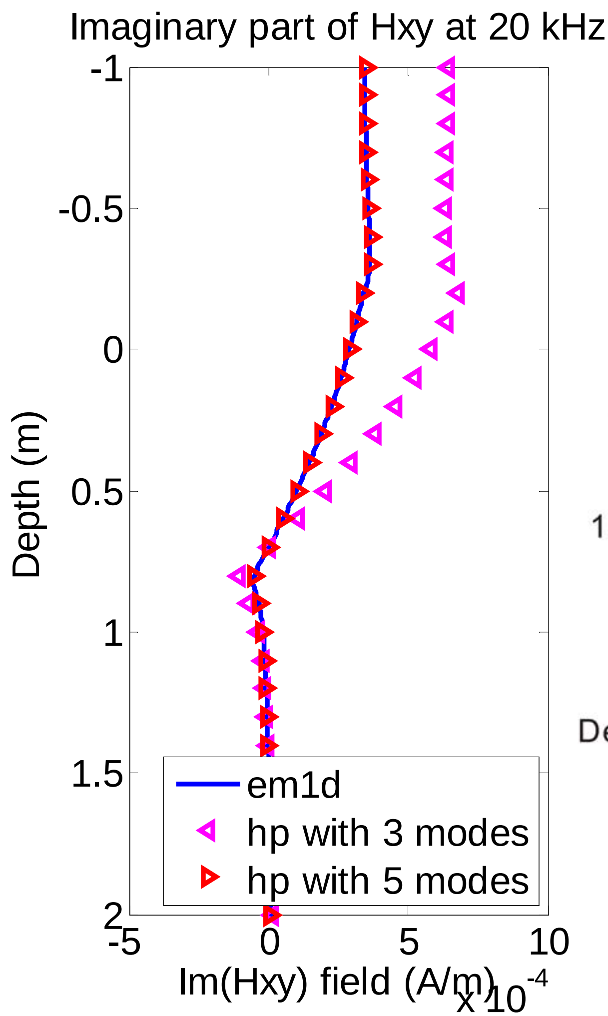


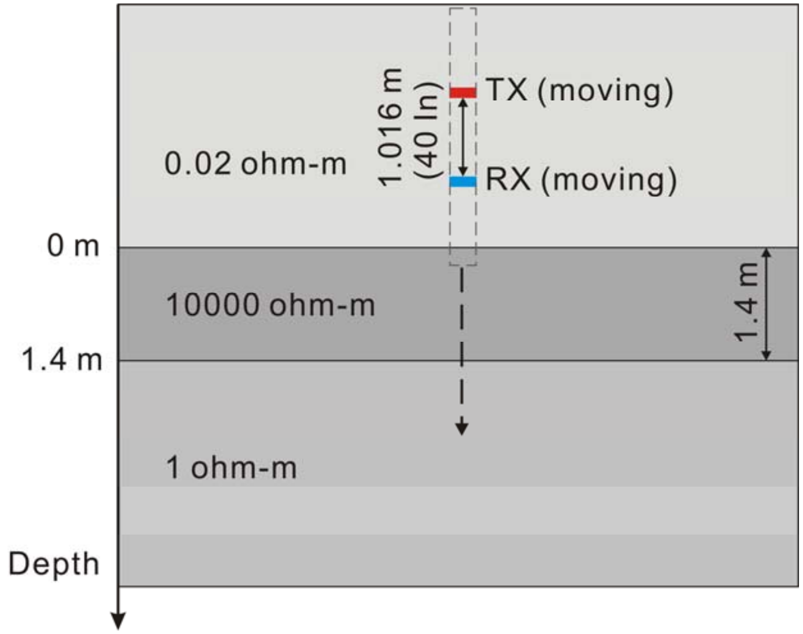


**Converged solutions with 5 Fourier modes**

# Verification of 2.5D Simulation ($H_{xz} = H_{zx}$)

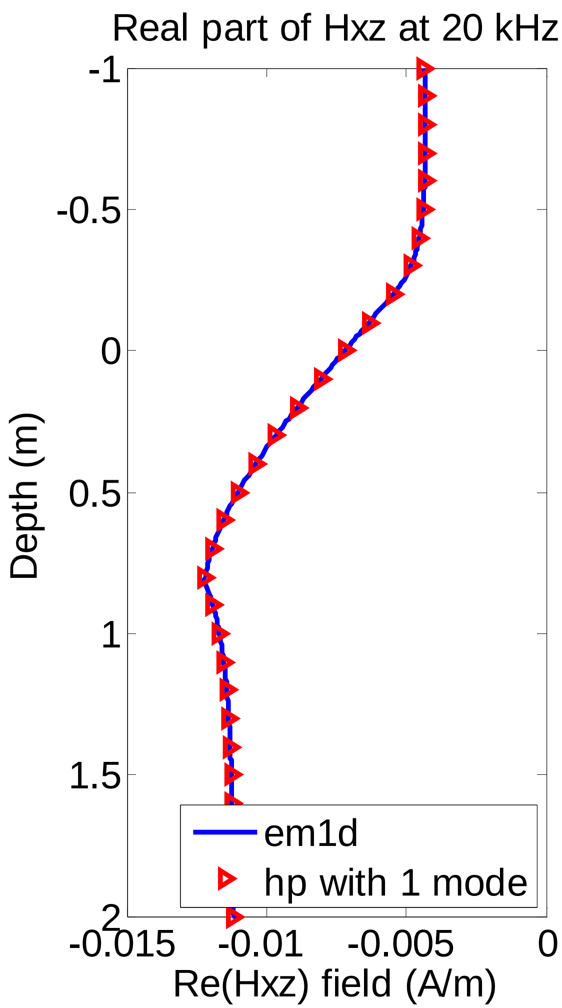


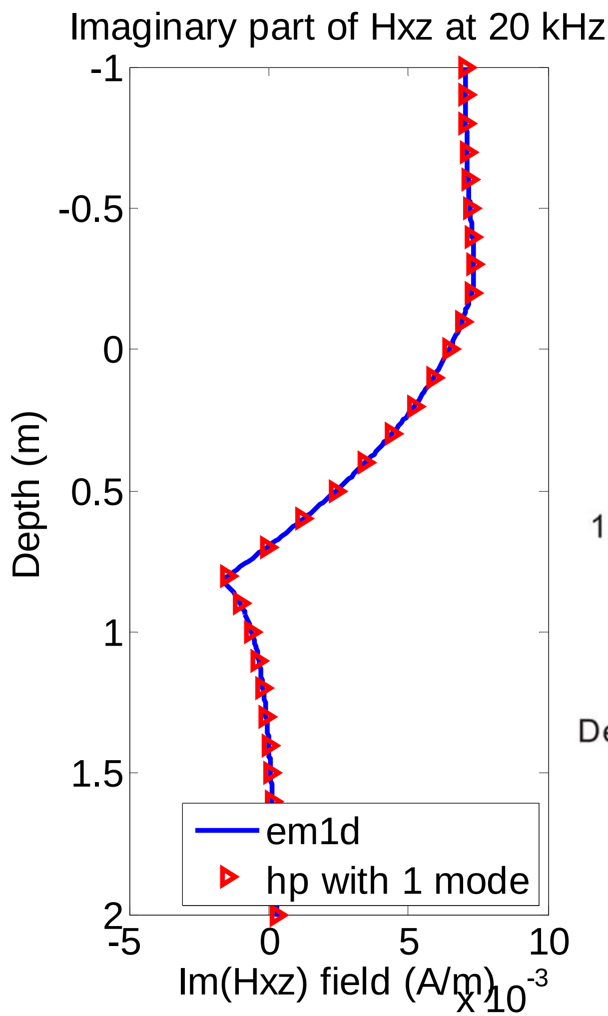


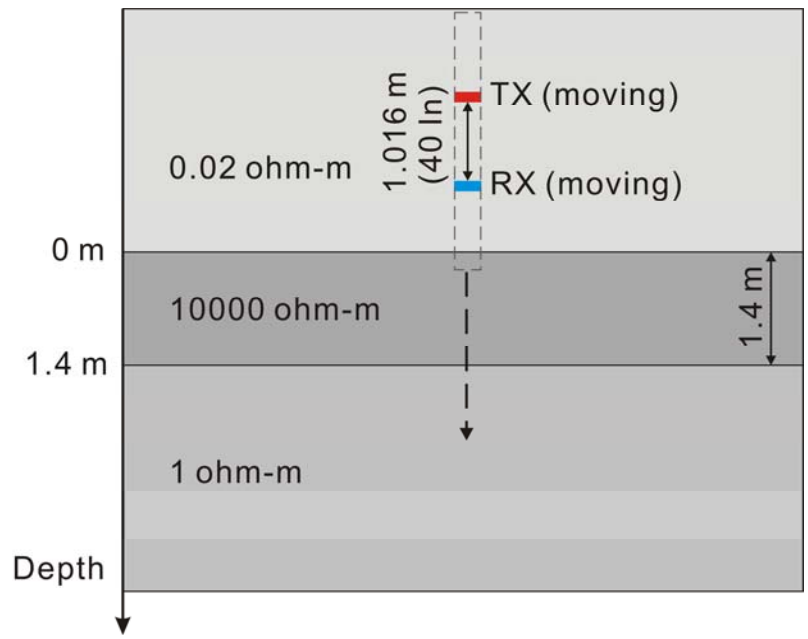


**The same solutions with 1 Fourier mode**

# Verification of 3D Simulation ($H_{xx} = H_{yy}$)

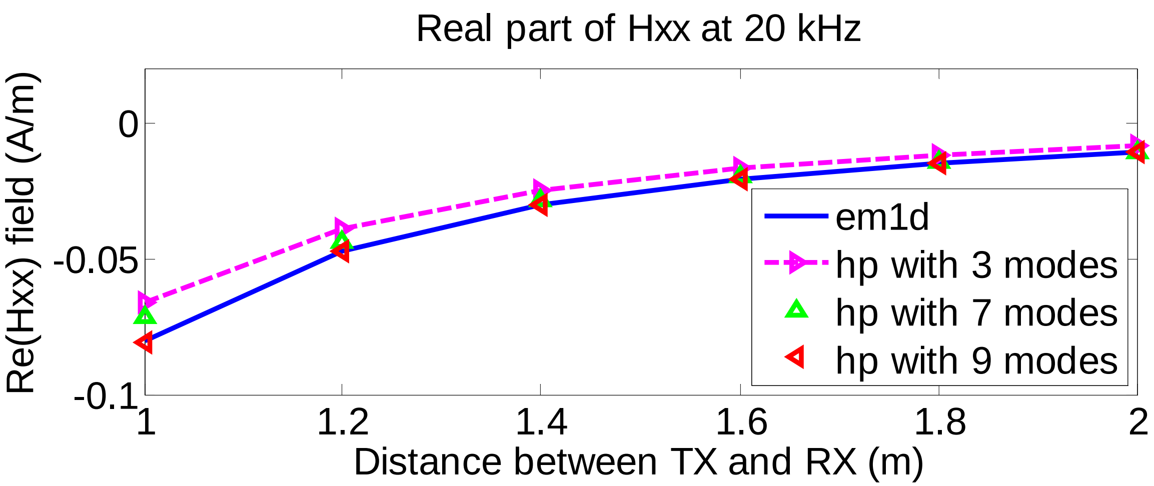


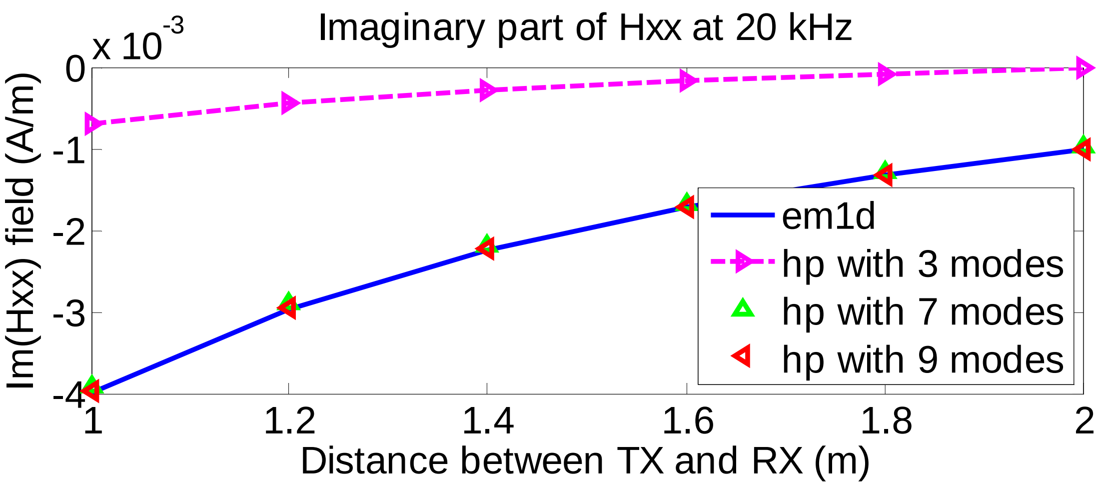


**Dip angle: 60 degrees**

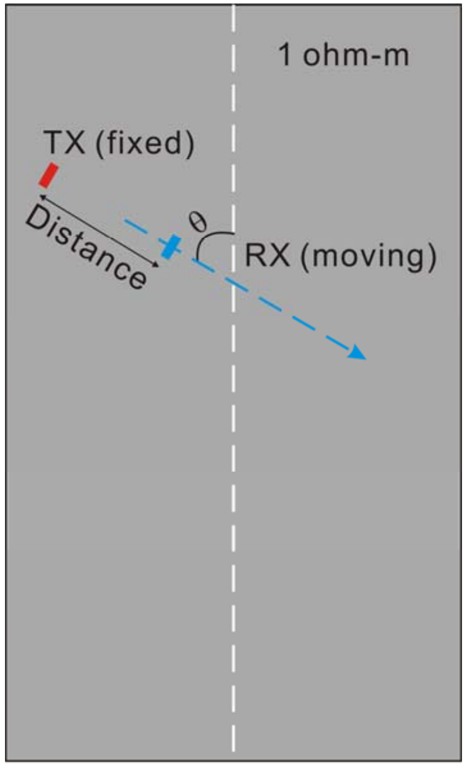


**Converged solutions with 9 Fourier mode**

# Verification of 3D Simulation ($H_{zz}$)

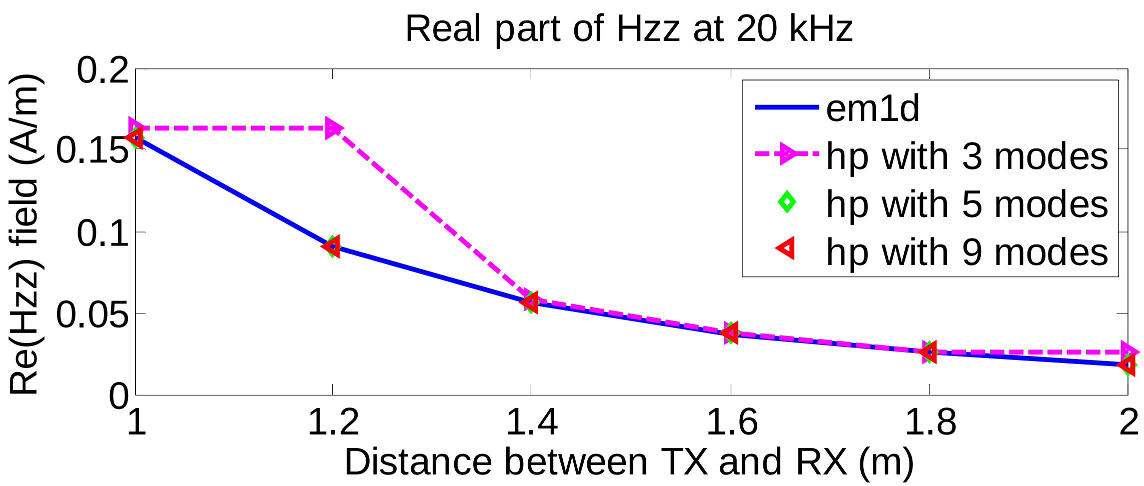


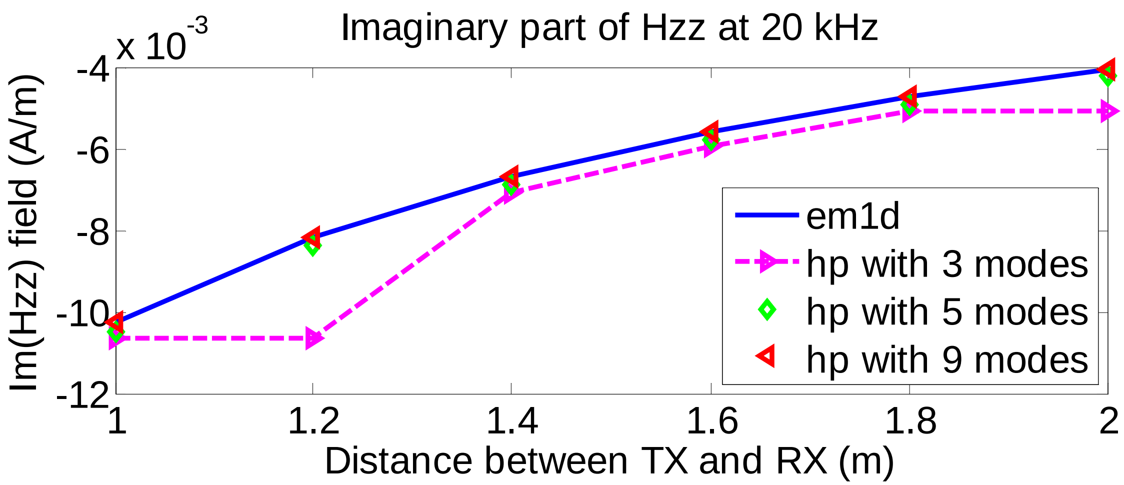


**Dip angle: 60 degrees**

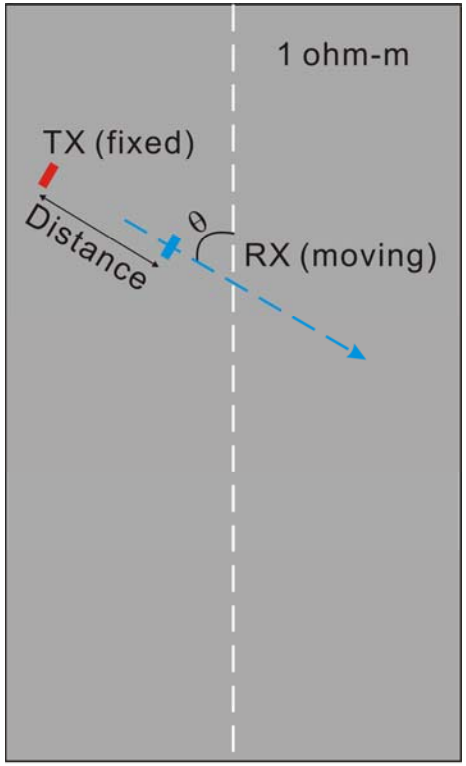


**Converged solutions with 5 Fourier mode**

# Description of the Tri-Axial Tool

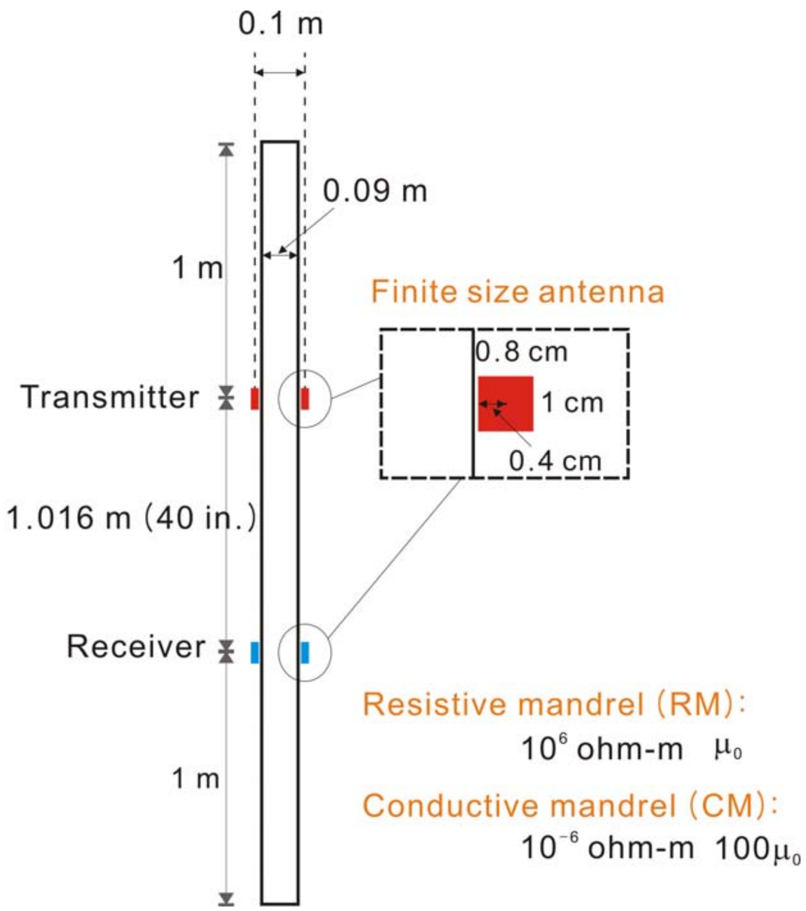


***Operating frequency: 20 kHz***

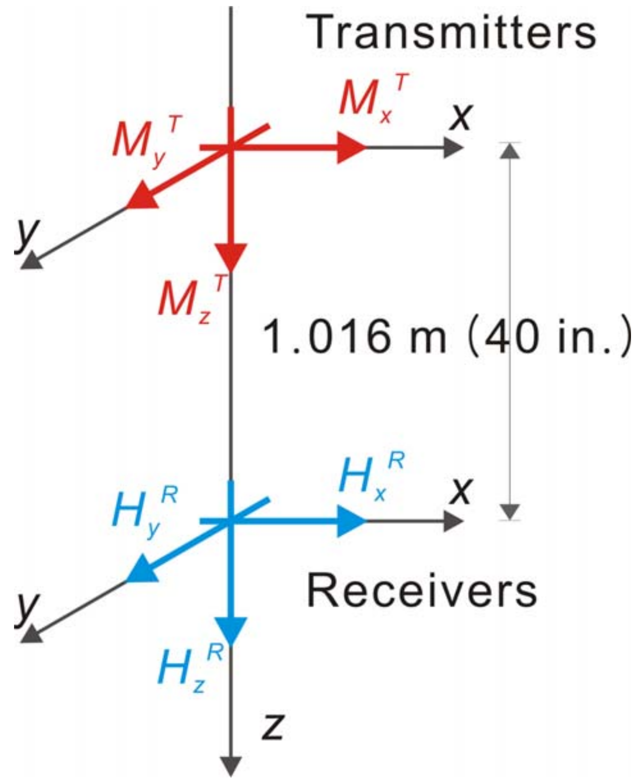

# Verification of 2.5D Simulation ($H_{xx}$)

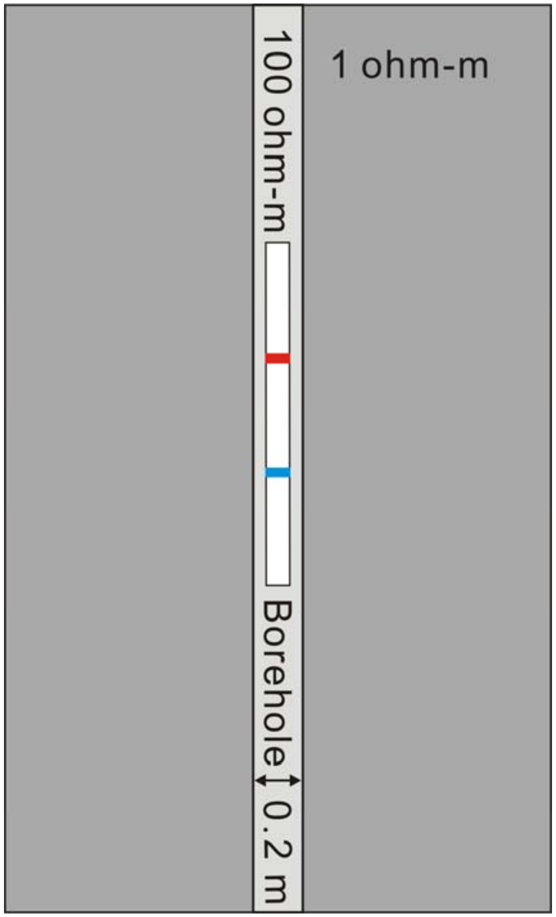


**Relative errors of tri-axial induction solutions with respect to the solution with 9 Fourier modes**

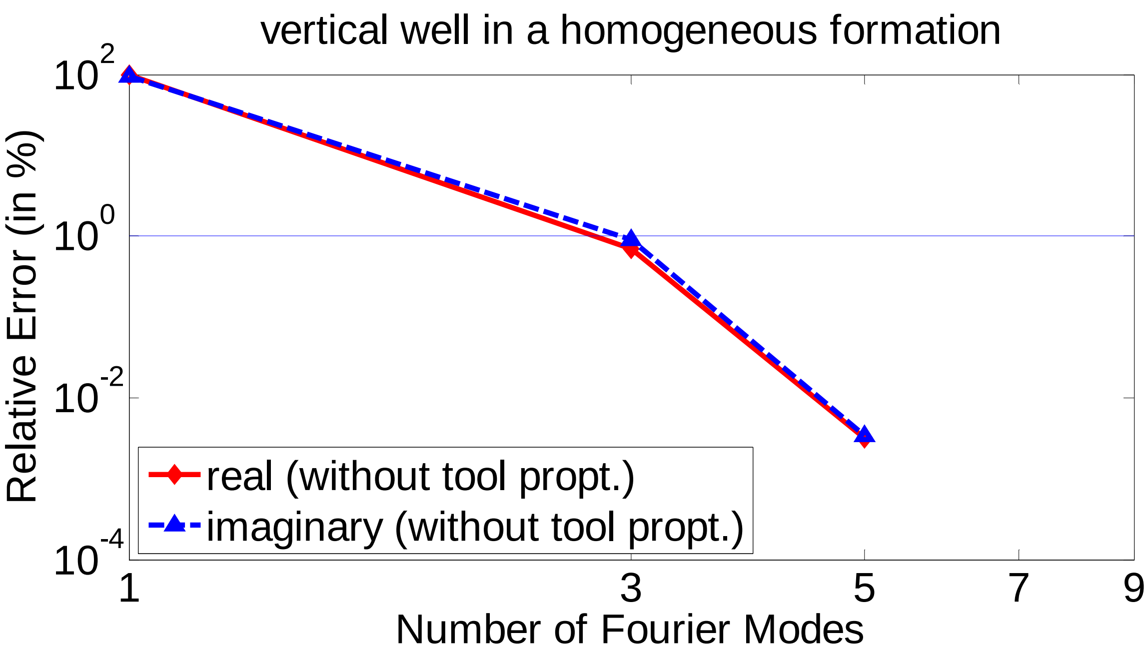

# Verification of 3D Simulation ($H_{xx}$)

**θ = 60 degrees**

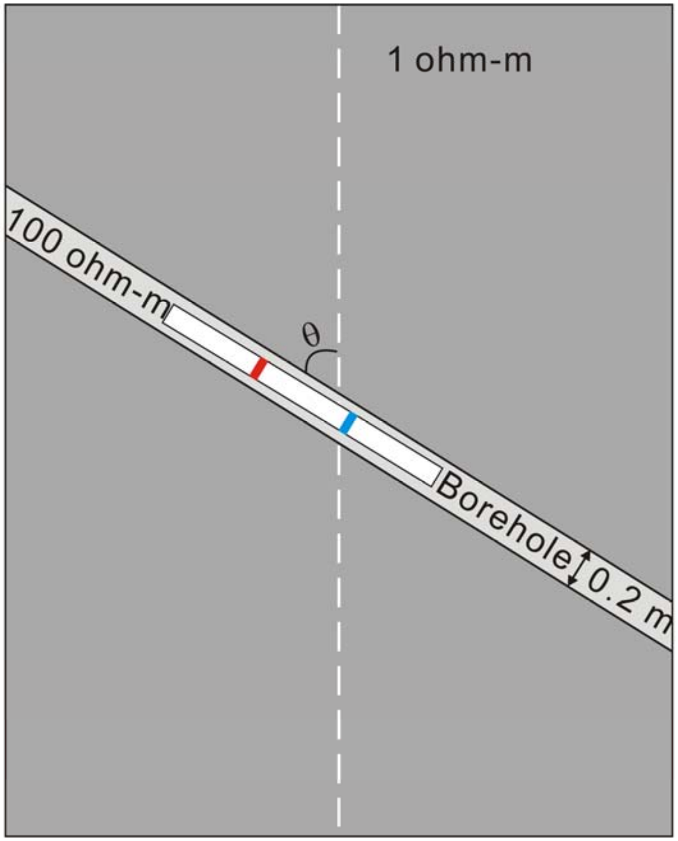


**Relative errors of tri-axial Induction solutions with respect to the solution for the vertical well**

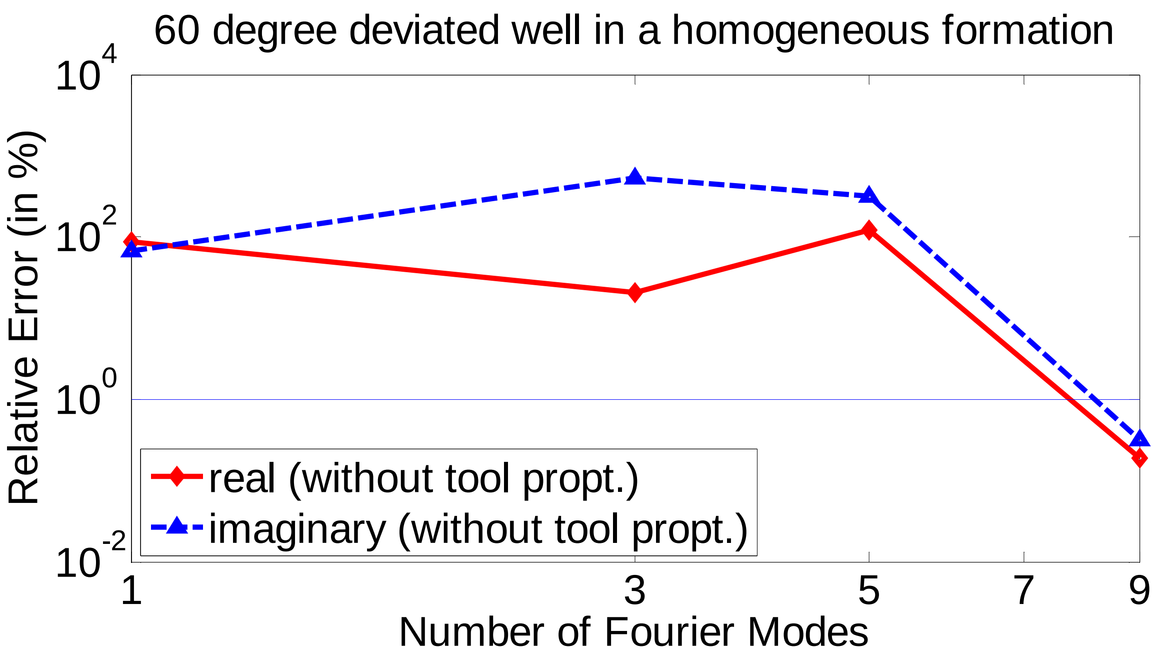

# Model for Experiments (Deviated Well)

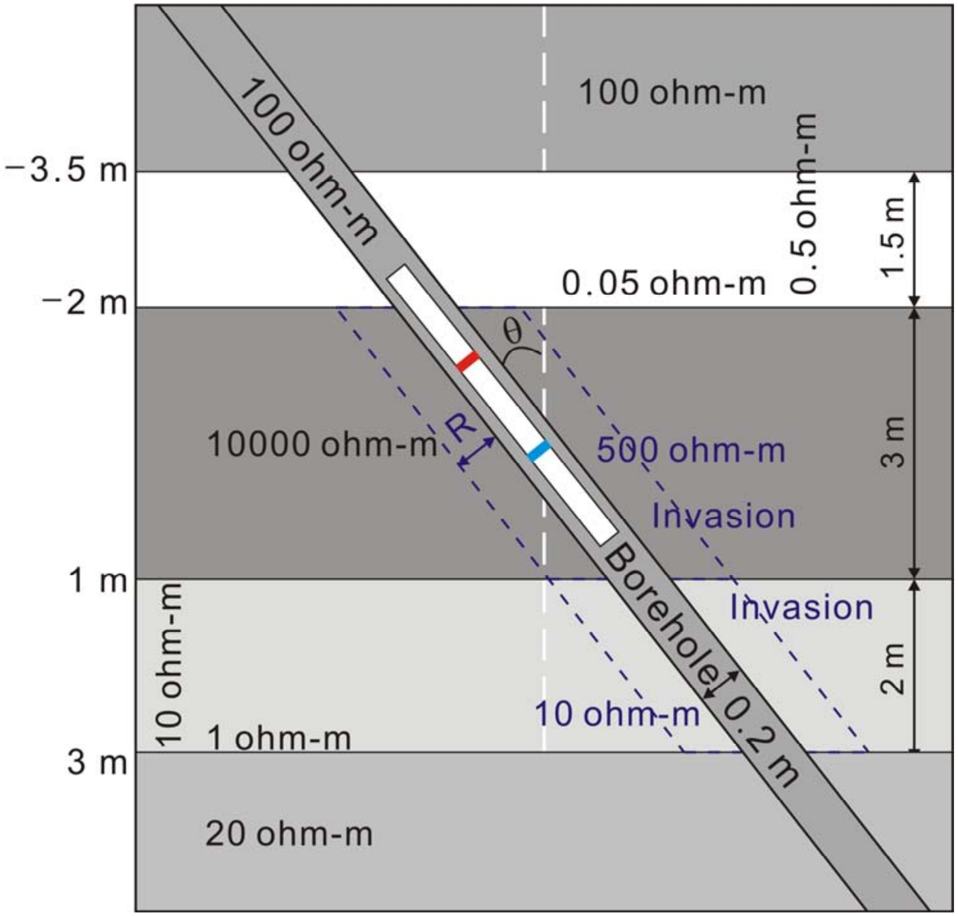


**Five layers: 100, 0.05, 10000, 1 and 20 ohm-m from top to bottom**

**Borehole: 0.1 m in radius**
**100 ohm-m in resistivity**

**$\theta$ = 0, 30 and 60 degrees**

**Resistive mandrel ($10^6$ ohm-m, $\mu_0$)**

**Invasion in the third and fourth layers**

**Anisotropy in the second and fourth layers**

# Convergence History of $H_{xx}$ in Vertical Well

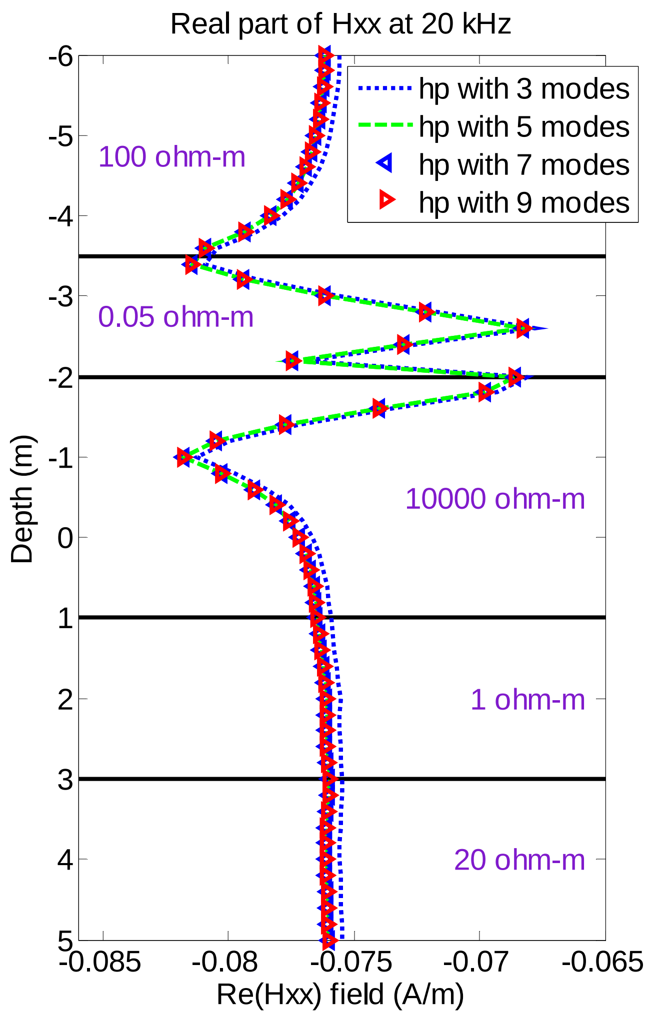


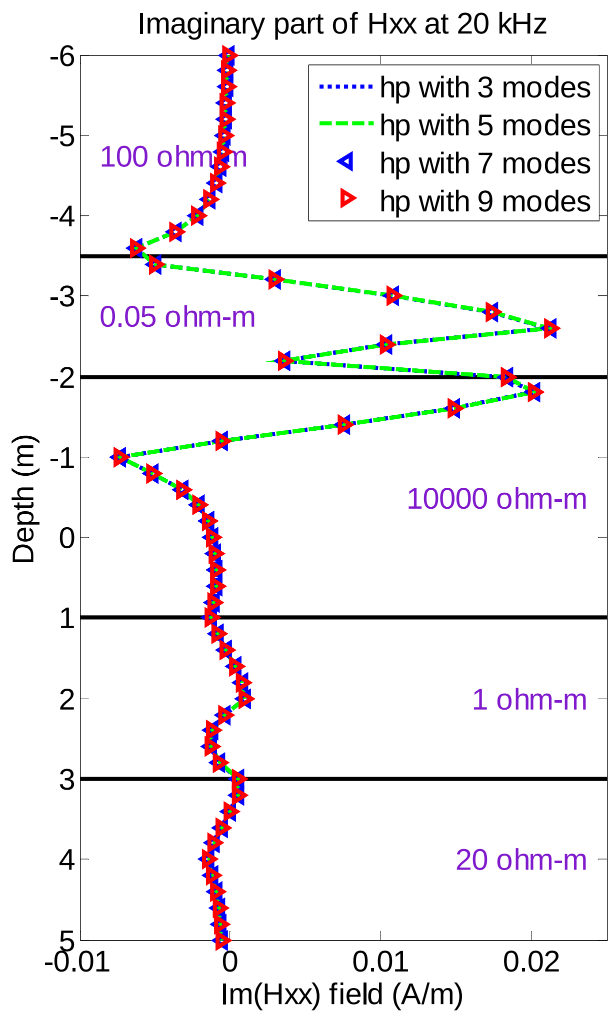


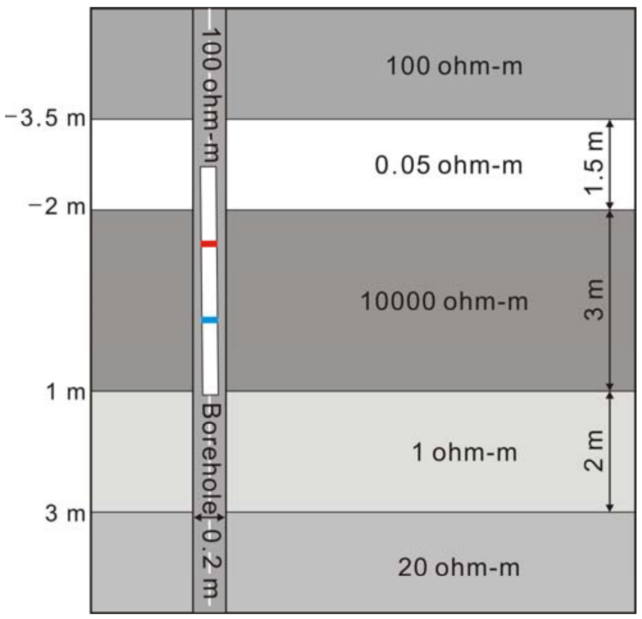


**Converged solutions with 5 Fourier modes**

# Convergence History of $H_{xx}$ in Deviated Well

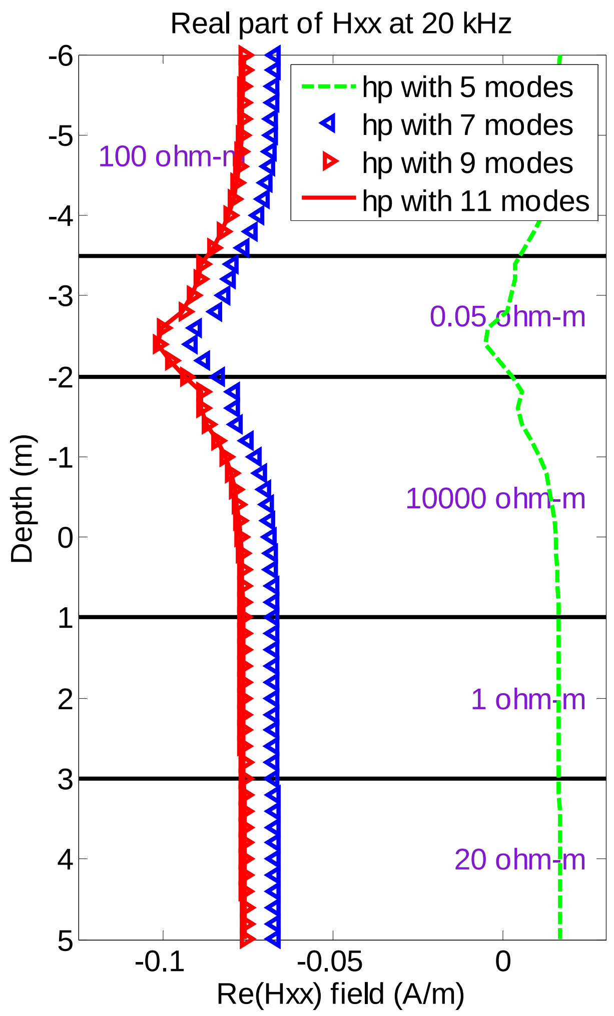


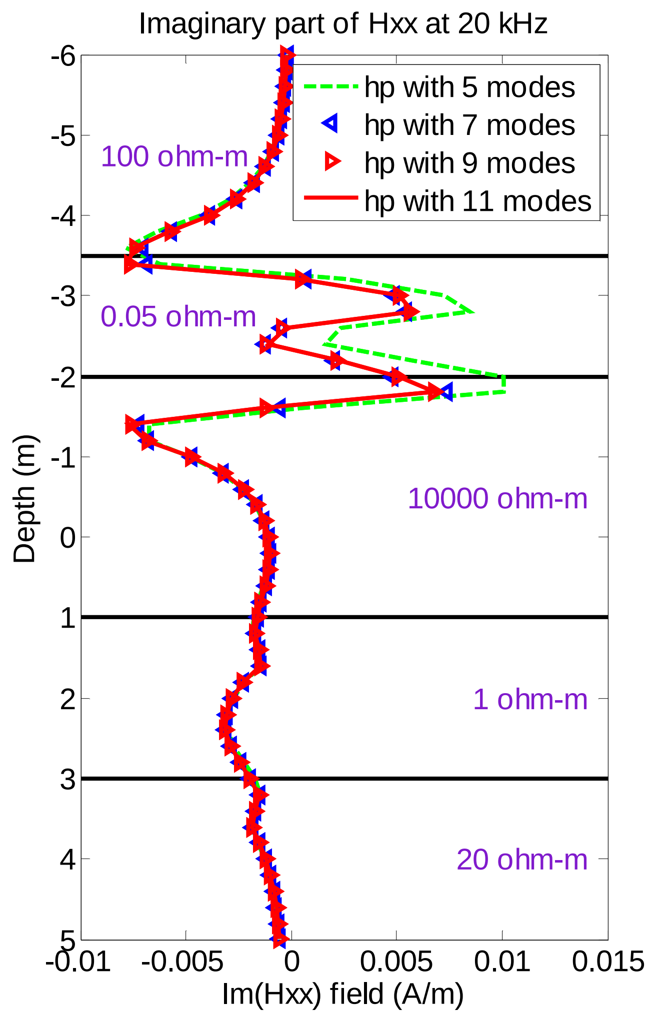


$\theta$ = 60 degrees

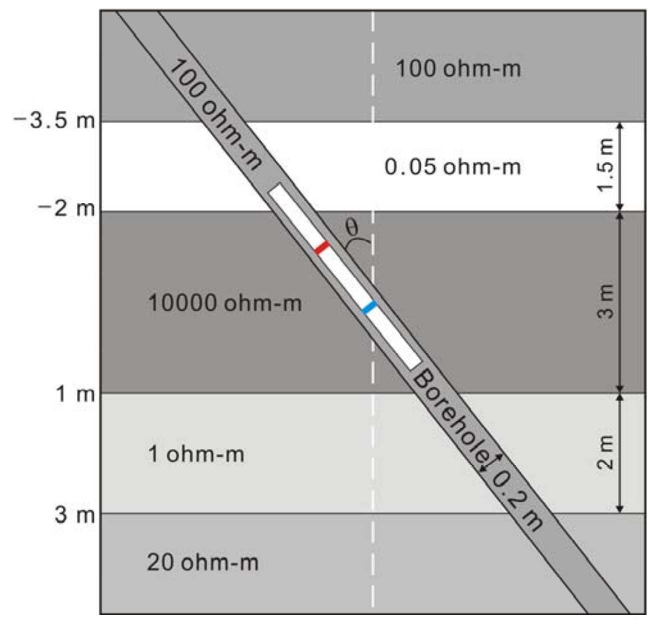


**Converged solutions with 9 Fourier modes**

# Deviated Wells (0, 30 & 60 degrees)

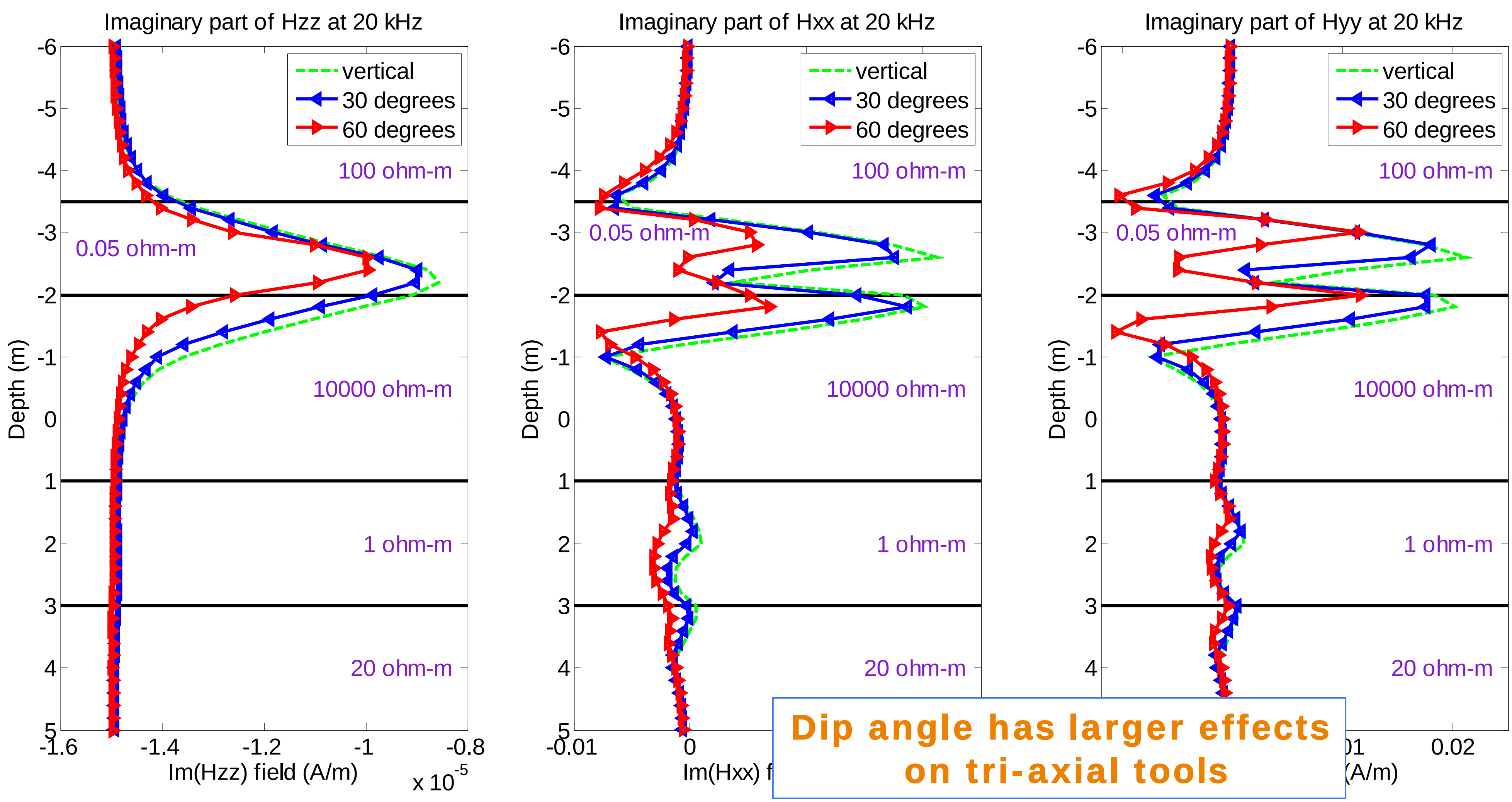


**Dip angle has larger effects on tri-axial tools**

# $H_{zz}$ in Deviated Wells with Invasion (Im.)

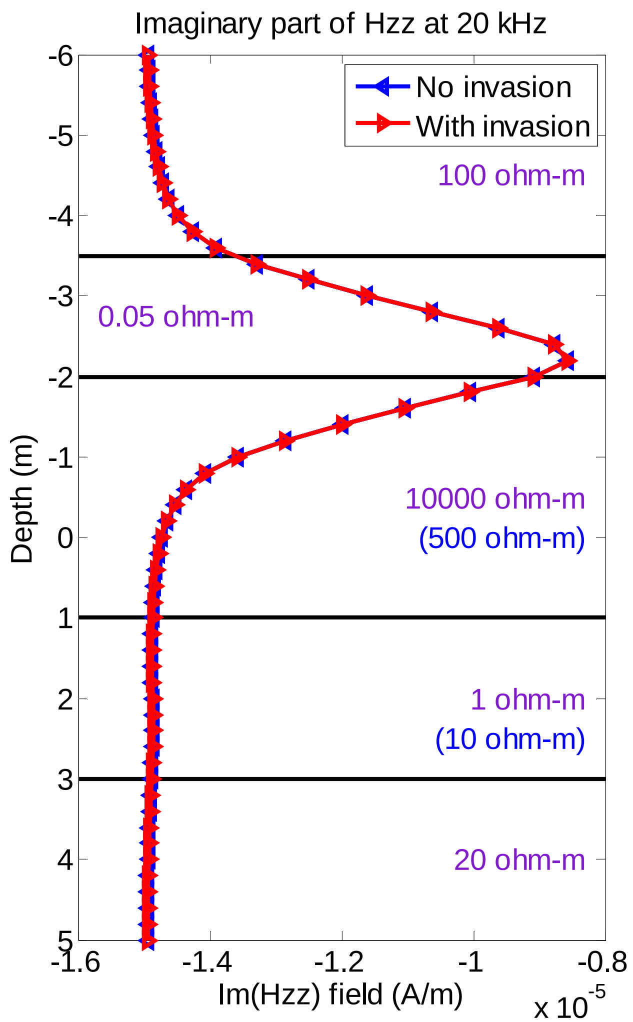


**vertical**

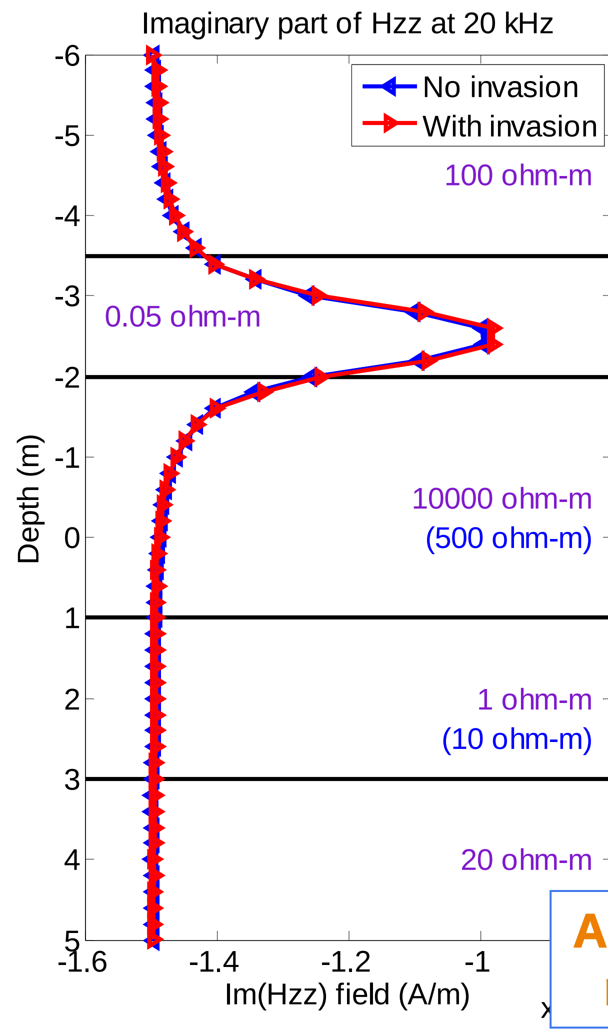


**60 degrees**

**Shallow invasion with R = 0.1 m**

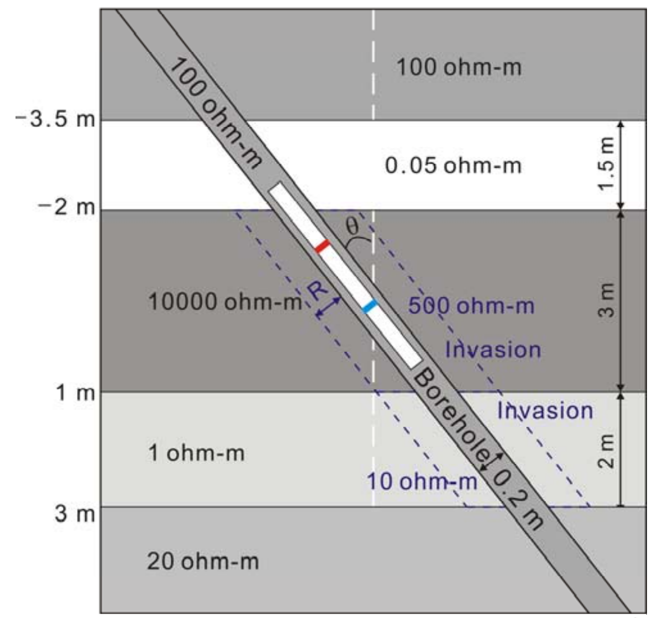


**Almost no effects of invasion regardless of the dip angle**

# $H_{xx}$ in Deviated Wells with Invasion (Im.)

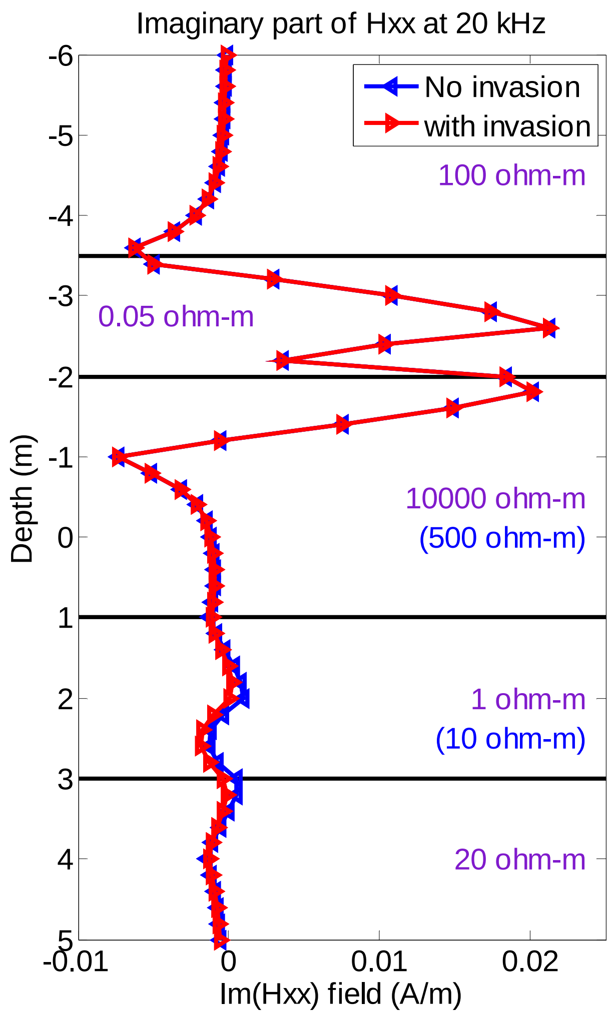


vertical

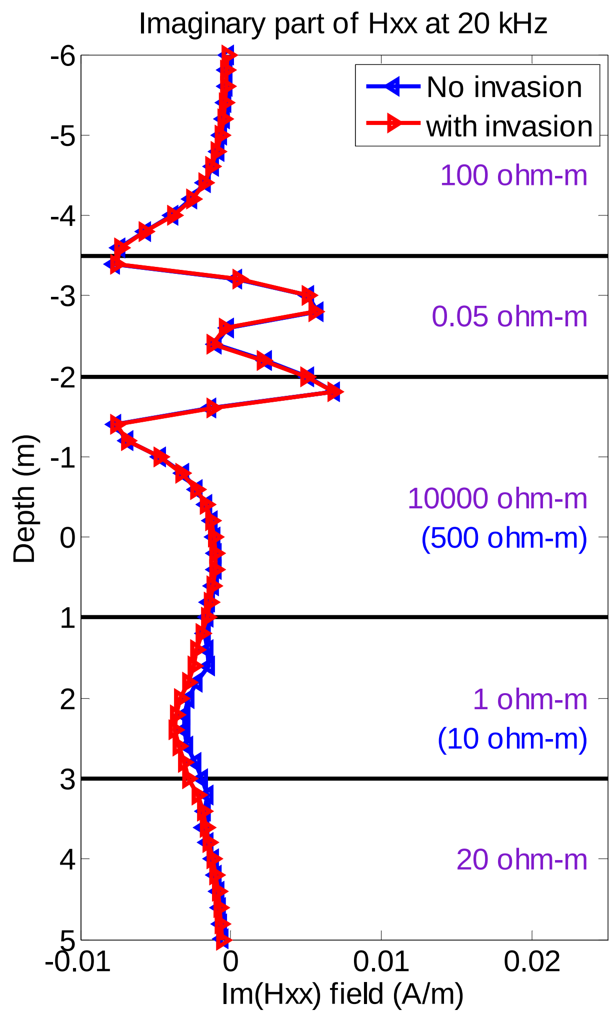


60 degrees

**Shallow invasion with R = 0.1 m**

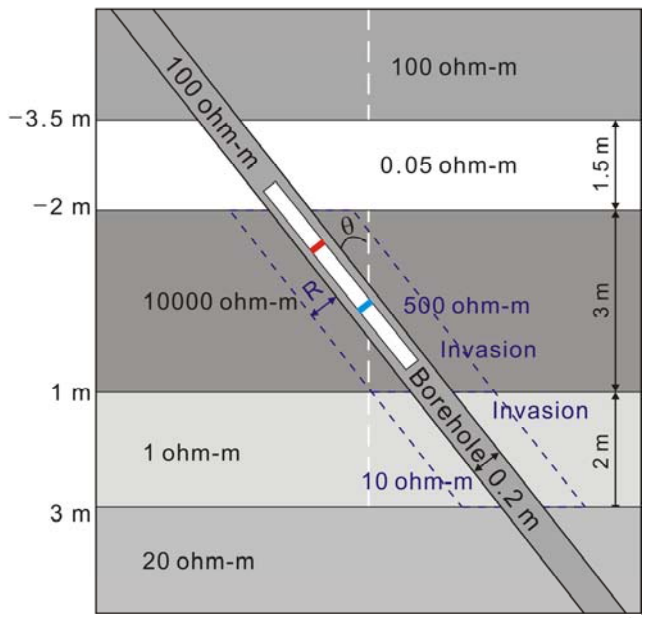


**Small effects of invasion**

# $H_{yy}$ in Deviated Wells with Invasion (Im.)

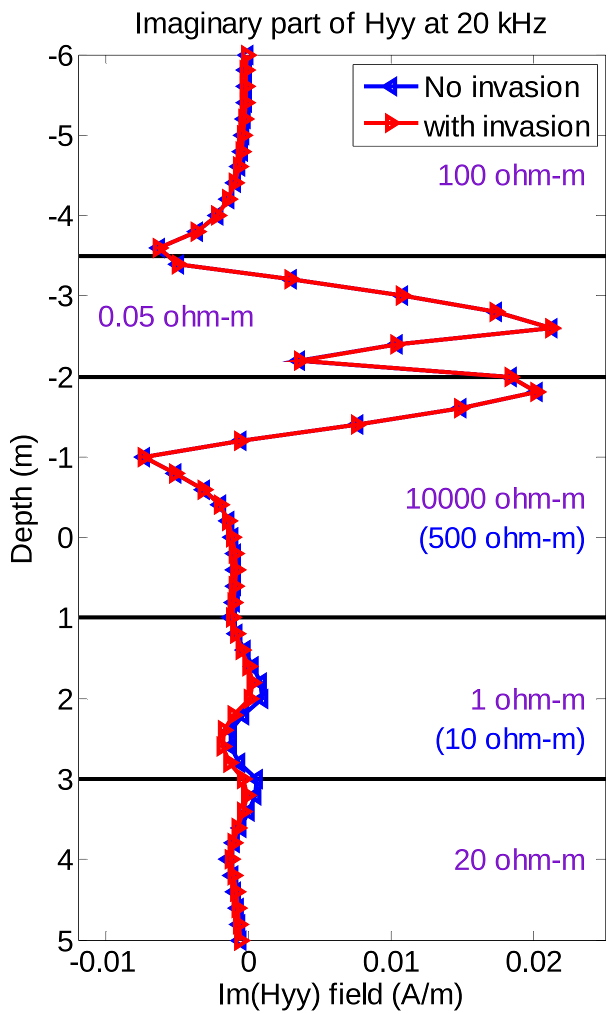


**vertical**

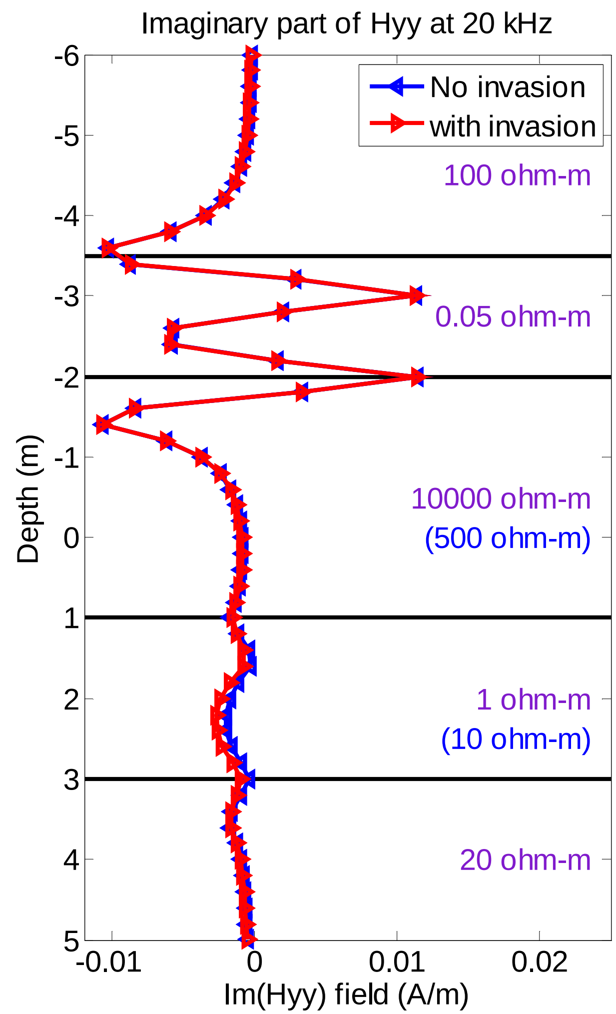


**60 degrees**

## Shallow invasion with R = 0.1 m

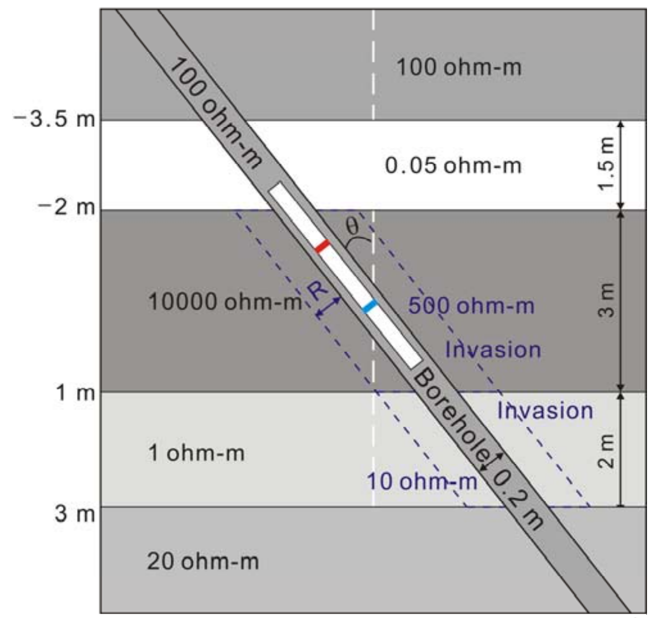


**Small effects of invasion**

# $H_{zz}$ in Deviated Wells with Anisotropy (Im.)

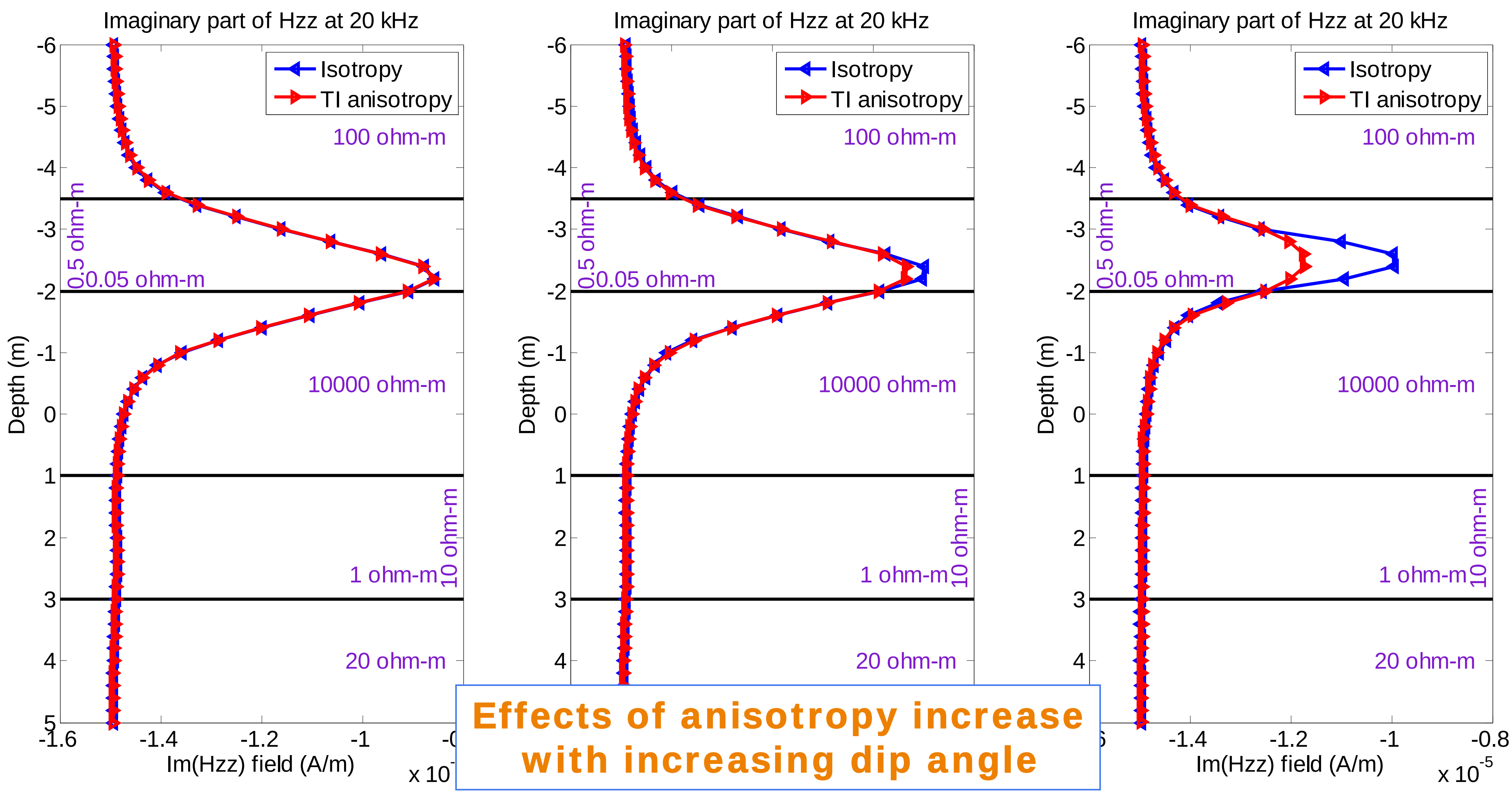


**Effects of anisotropy increase with increasing dip angle**

**vertical** **30 degrees** **60 degrees**

# $H_{xx}$ in Deviated Wells with Anisotropy (Im.)

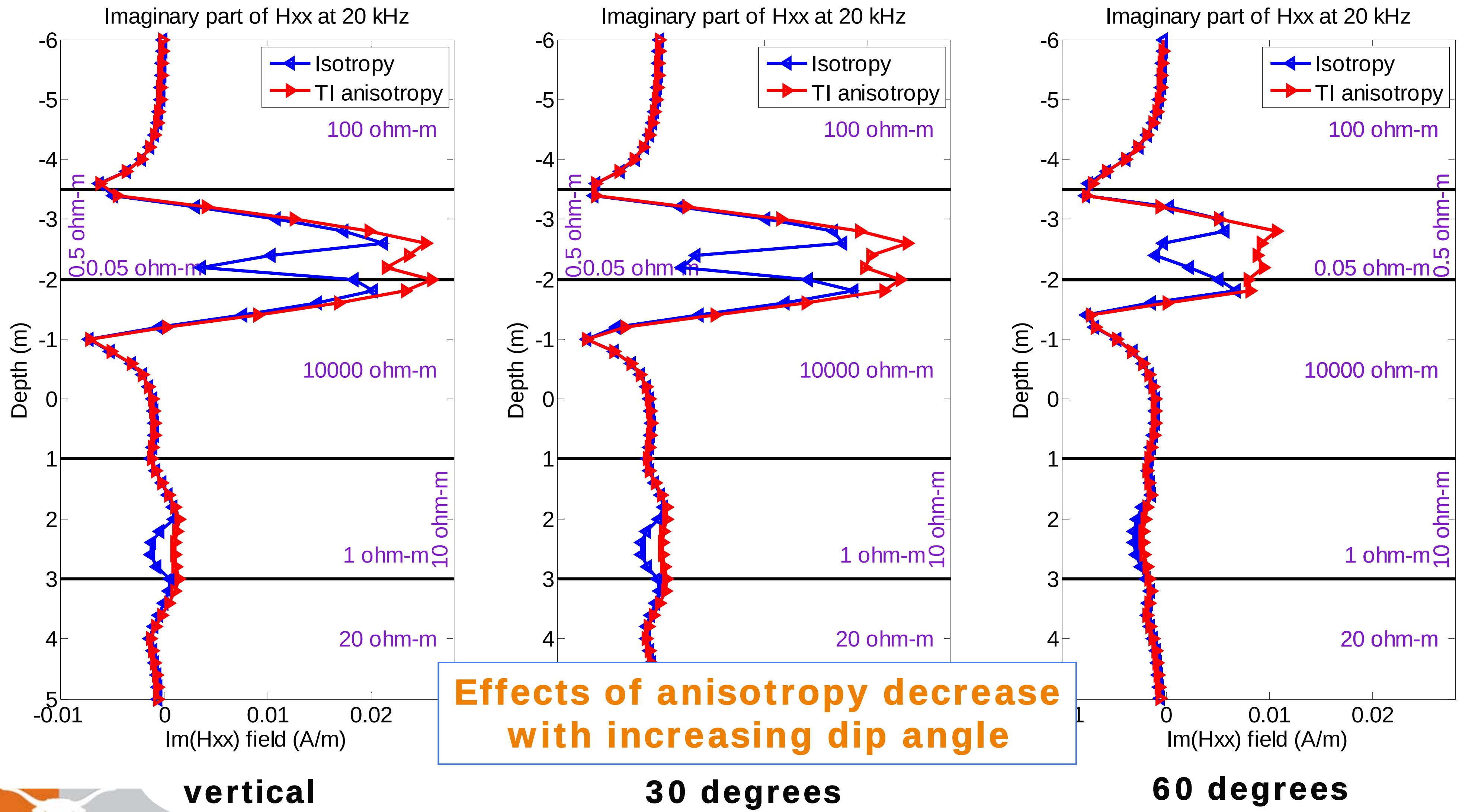


**Effects of anisotropy decrease with increasing dip angle**

# $H_{yy}$ in Deviated Wells with Anisotropy (Im.)

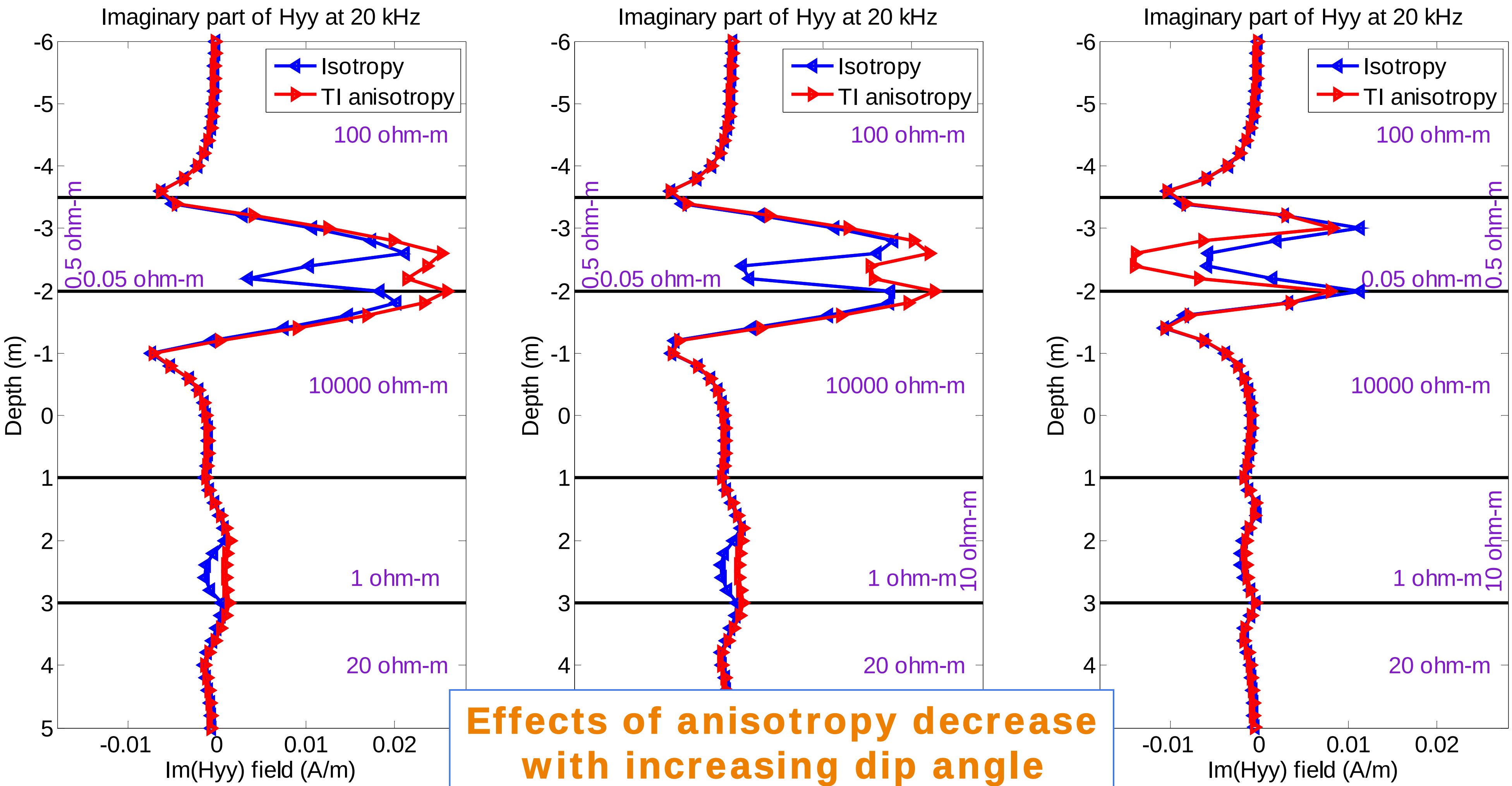


**Effects of anisotropy decrease with increasing dip angle**

**vertical** | **30 degrees** | **60 degrees**

# $H_{xx}$ at 20 KHz and 2 MHz in Vertical Well

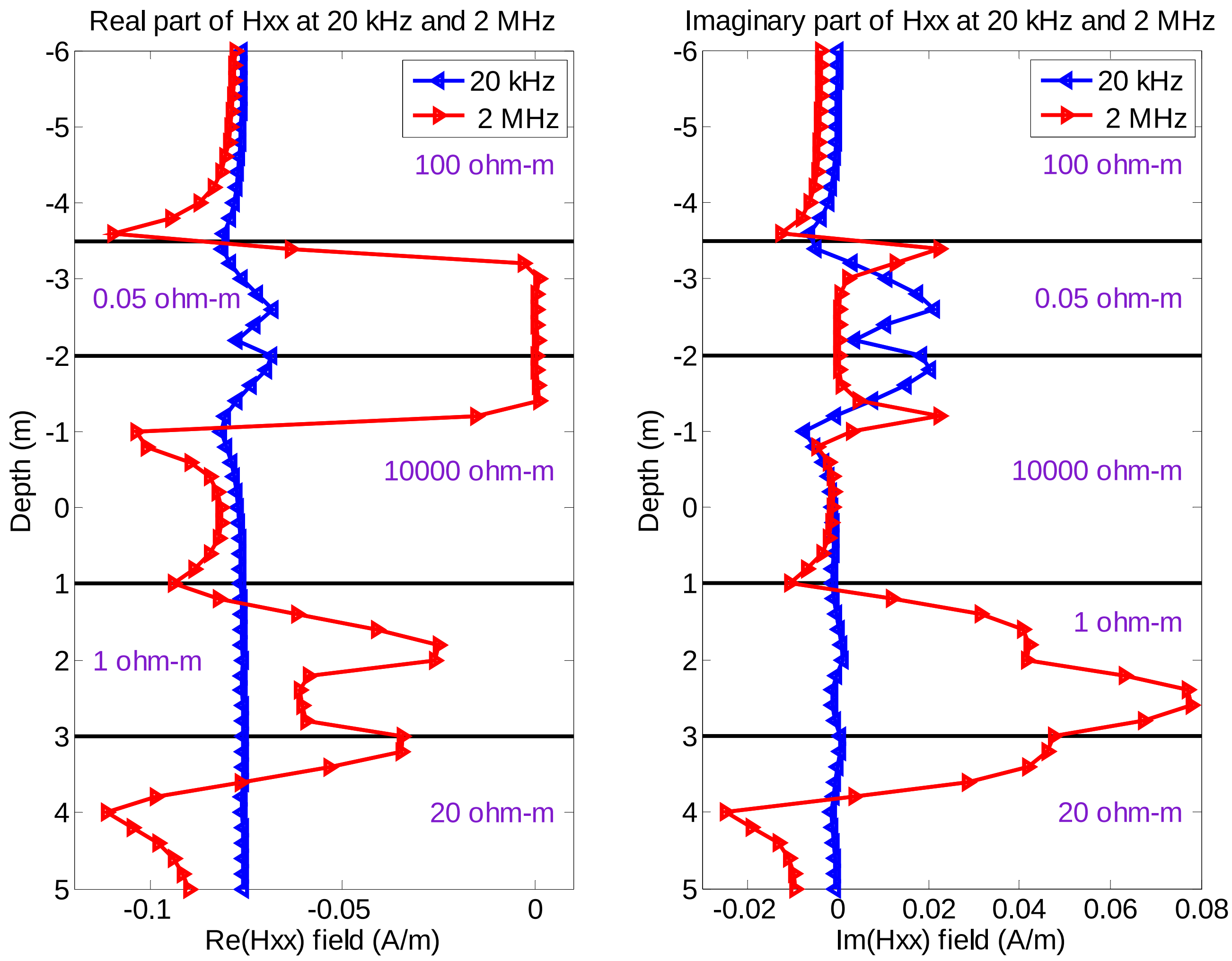


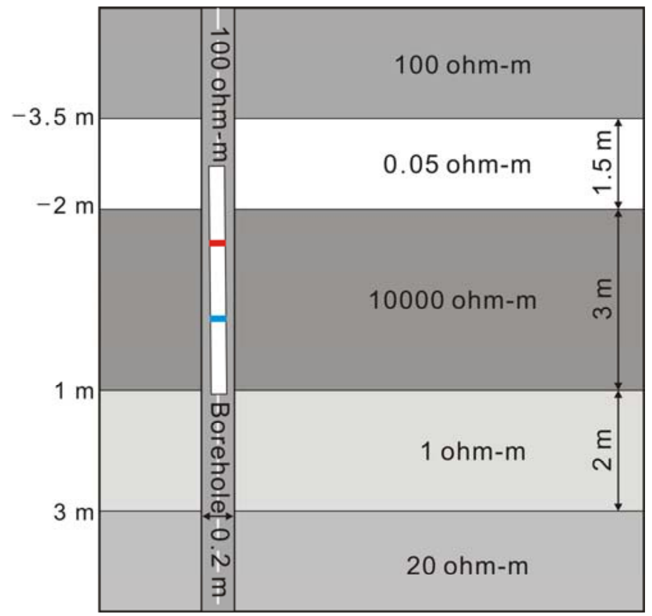


**Larger variations at 2 MHz than at 20 kHz**

# Model for Experiments (Eccentered Tool)

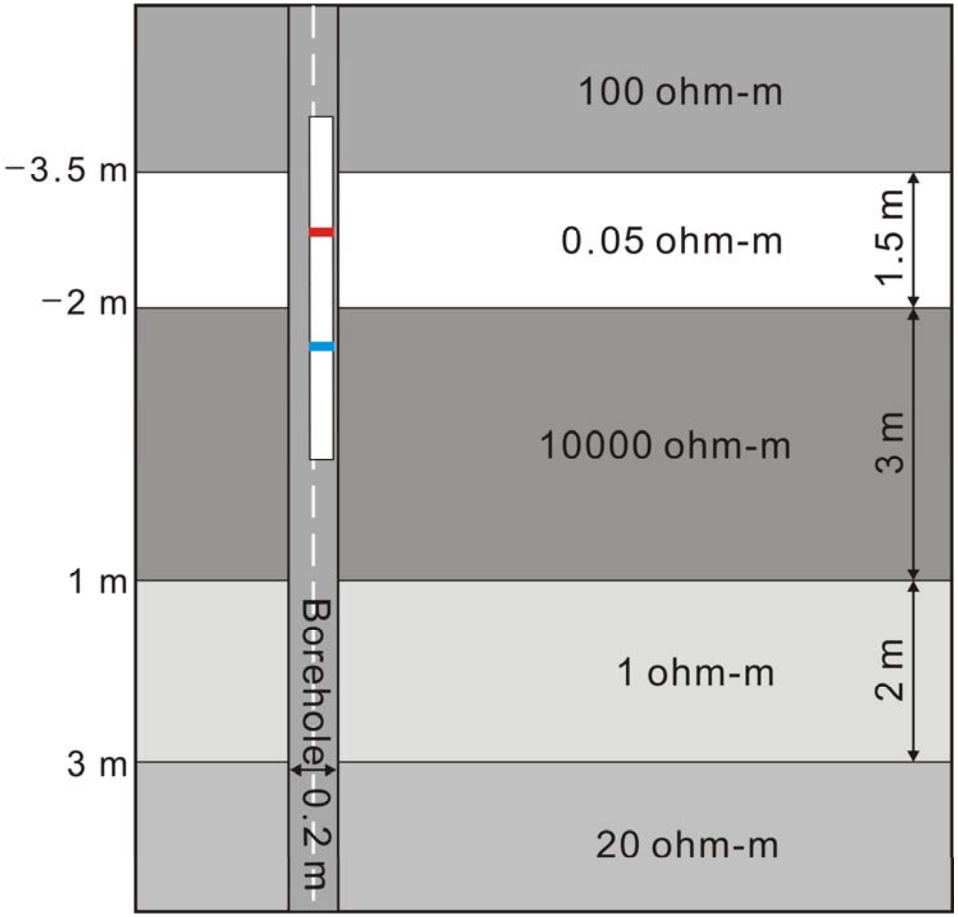


**Five layers: 100, 0.05, 10000, 1 and 20 ohm-m from top to bottom**

**Radius of borehole: 0.1 m**

# Model for Experiments (Eccentered Tool)

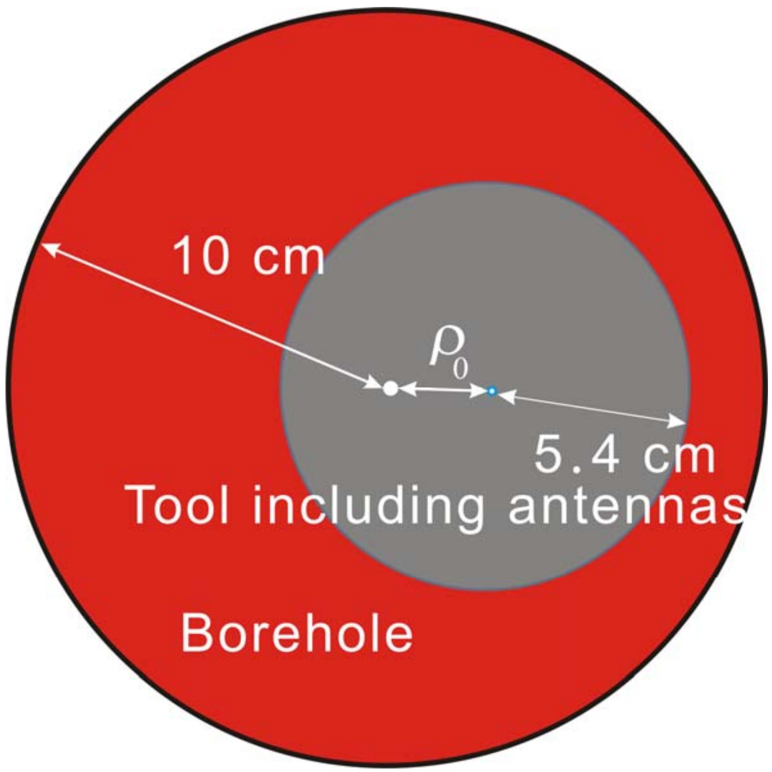


Five layers: 100, 0.05, 10000, 1 and 20 ohm-m from top to bottom

Radius of borehole: 0.1 m

Conductive borehole (CB): 1 ohm-m

Resistive borehole (RB) : 1000 ohm-m

Conductive mandrel (CM): $10^{-6}$ ohm-m, $100\mu_0$

Resistive mandrel (RM): $10^{6}$ ohm-m, $\mu_0$

Eccentered distance ($\rho_0$): 0, 0.45, 2.25, 3.15 cm

# $H_{zz}$ ($\rho_0$: 0, 0.45, 2.25, 3.15 cm)

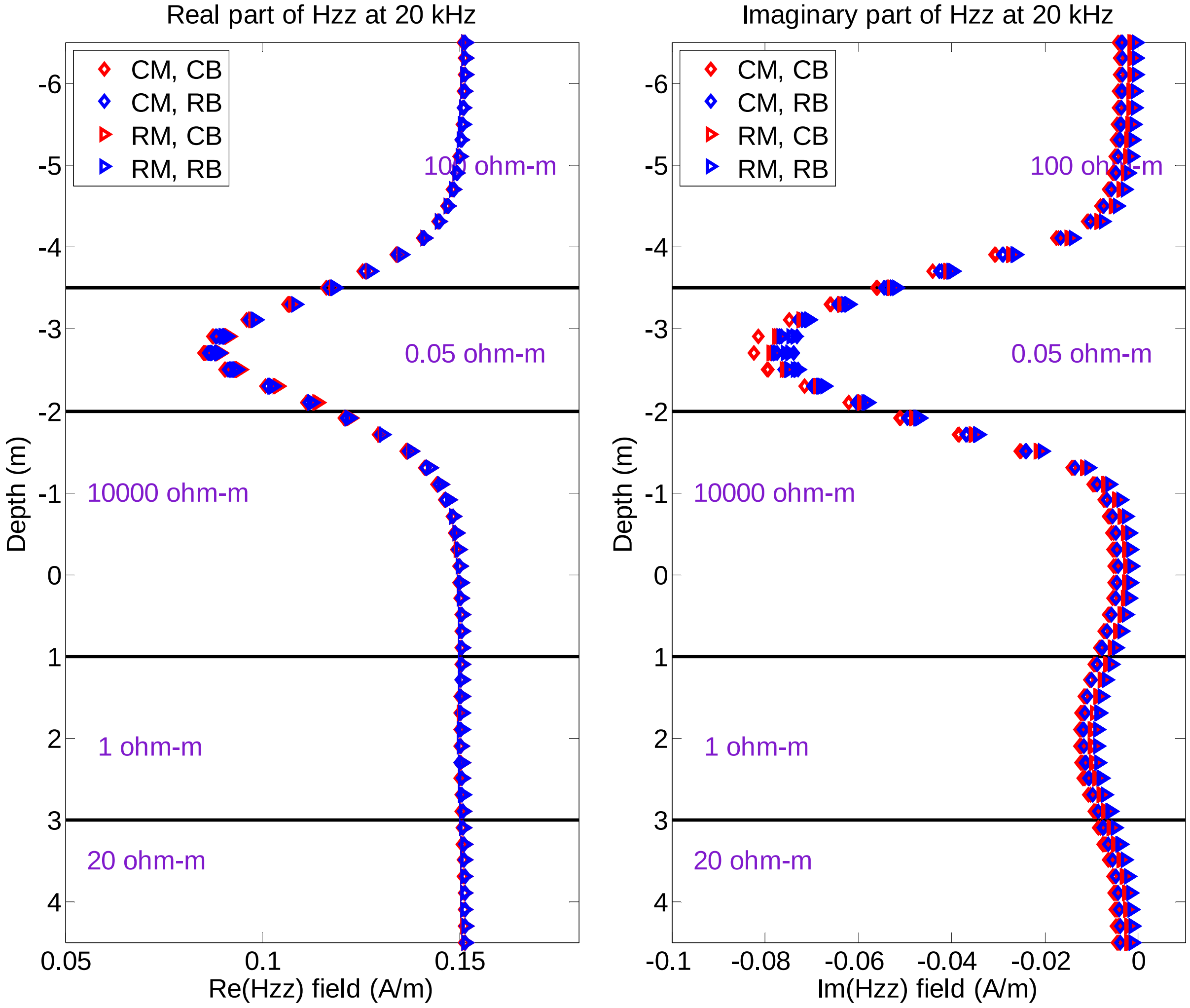


CM: Conductive Mandrel ($10^{-6}$ ohm-m, $100\mu_0$)

RM: Resistive Mandrel ($10^{6}$ ohm-m)

CB: Conductive Borehole (1 ohm-m)

RB: Resistive Borehole ($10^{3}$ ohm-m)

**No big difference between results with RM and CM**

**Slight deviations in results with RM**

# $H_{zz}$ ($\rho_0$: 0, 0.45, 2.25, 3.15 cm)

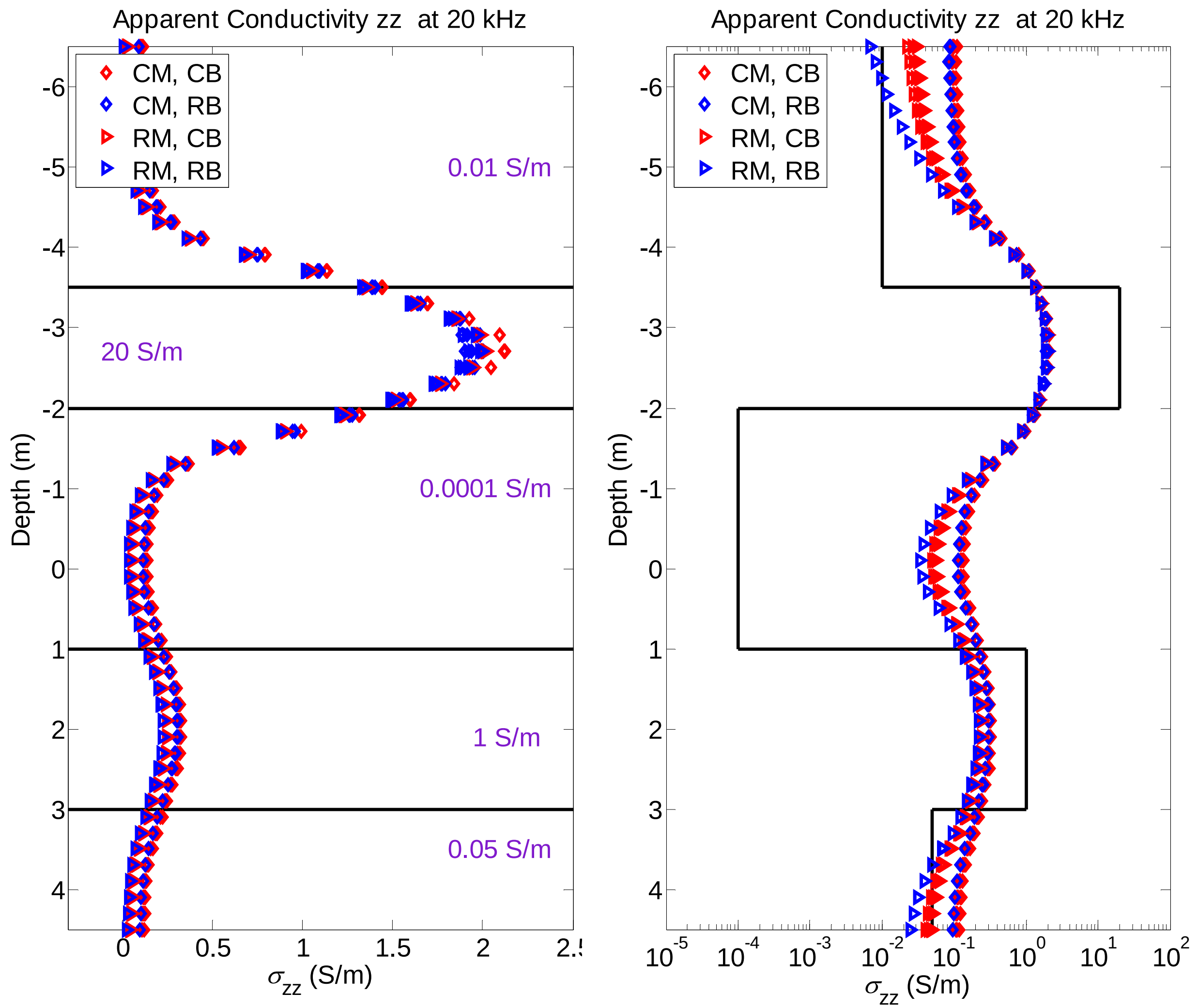


CM: Conductive Mandrel ($10^{-6}$ ohm-m, $100\mu_0$)

RM: Resistive Mandrel ($10^{6}$ ohm-m)

CB: Conductive Borehole (1 ohm-m)

RB: Resistive Borehole ($10^{3}$ ohm-m)

**No big difference between results with RM and CM**

**Slight deviations in results with RM**

# $H_{xx}$ ($\rho_0$: 0, 0.45, 2.25, 3.15 cm)

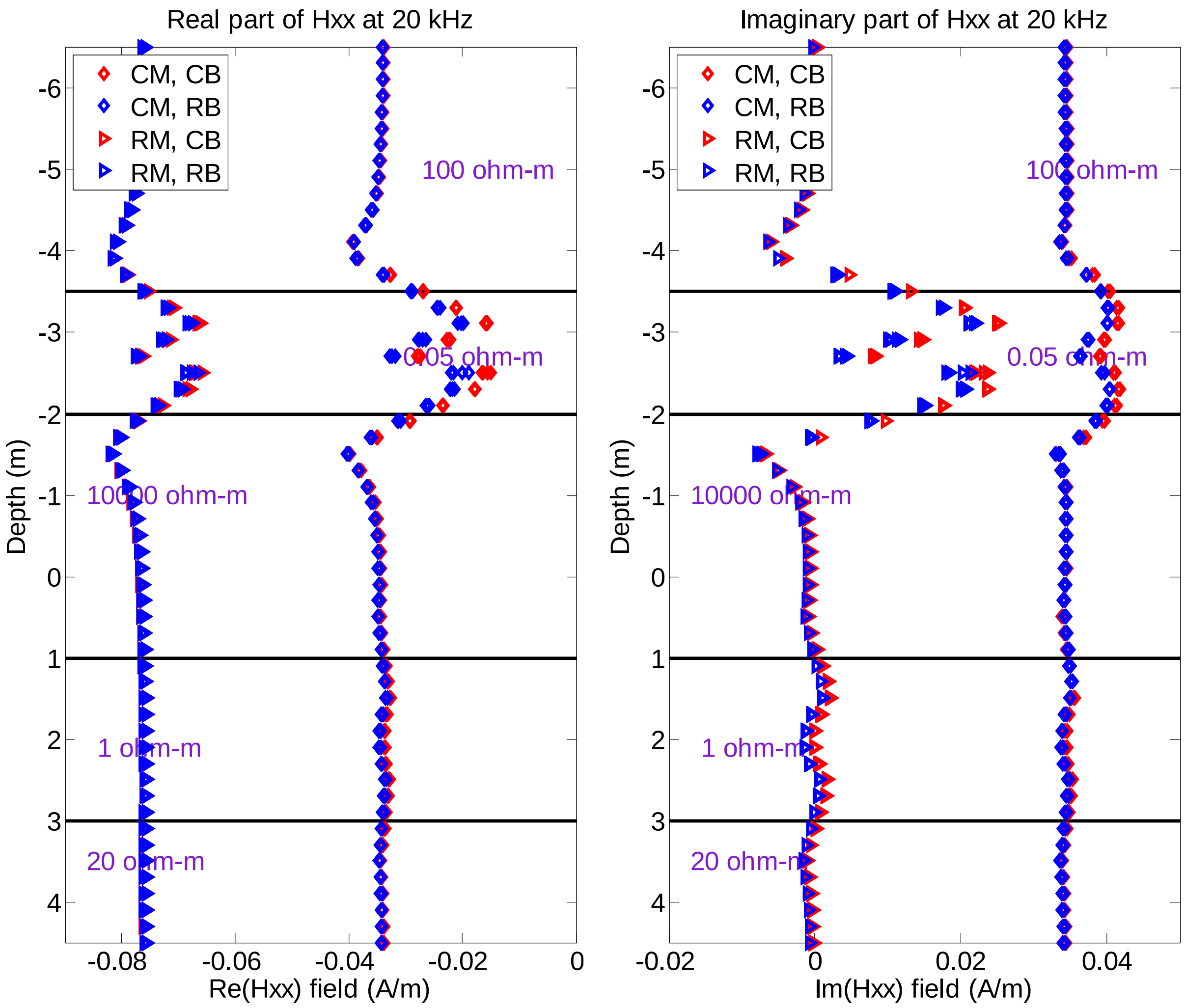


CM: Conductive Mandrel ($10^{-6}$ ohm-m, $100\mu_0$)

RM: Resistive Mandrel ($10^{6}$ ohm-m)

CB: Conductive Borehole (1 ohm-m)

RB: Resistive Borehole ($10^{3}$ ohm-m)

**Different results between RM and CM**

**More deviations in results with RM**

# $H_{xx}$ ($\rho_0$: 0, 0.45, 2.25, 3.15 cm)

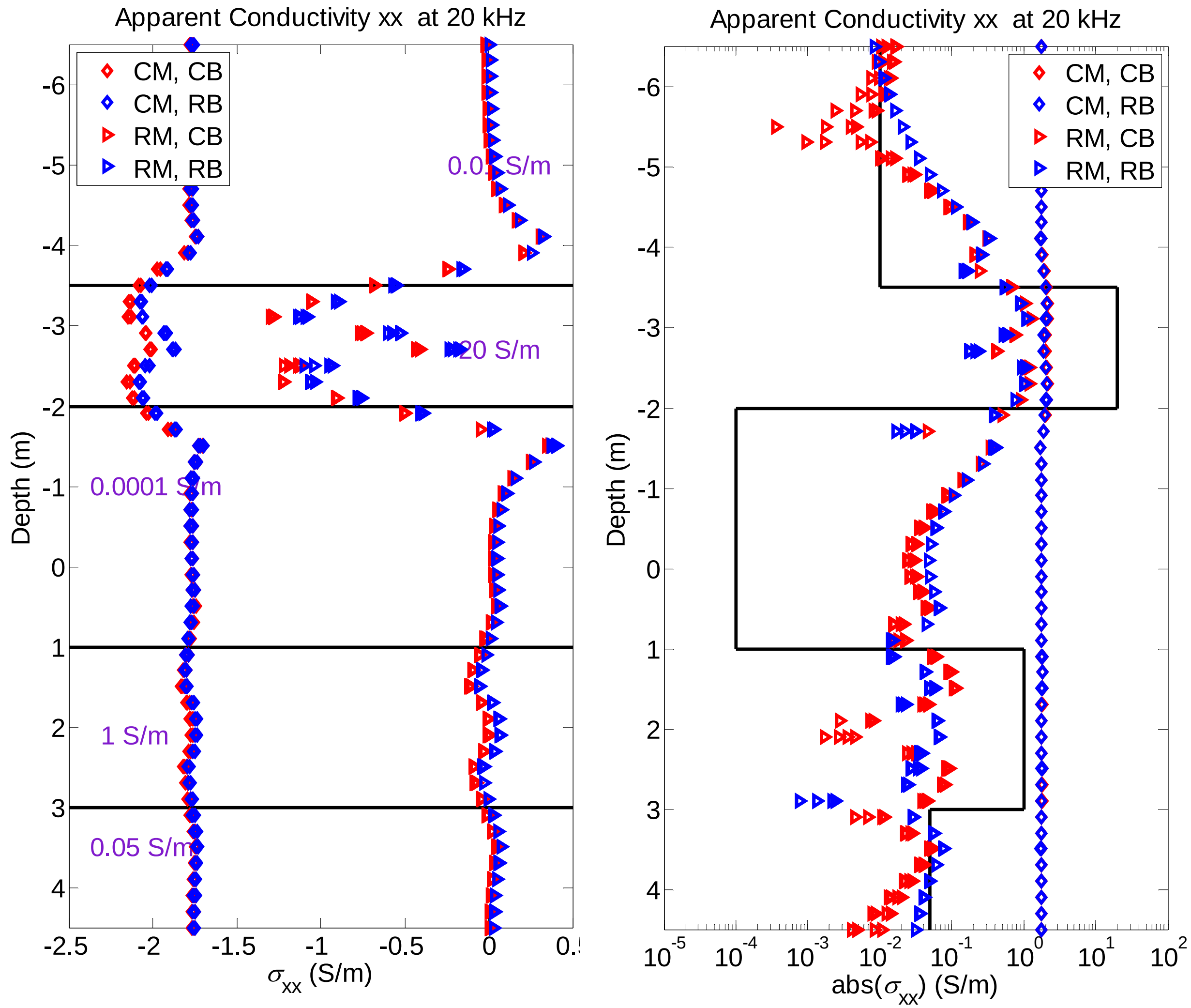


CM: Conductive Mandrel ($10^{-6}$ ohm-m, $100\mu_0$)

RM: Resistive Mandrel ($10^{6}$ ohm-m)

CB: Conductive Borehole (1 ohm-m)

RB: Resistive Borehole ($10^{3}$ ohm-m)

**Different results between RM and CM**

**More deviations in results with RM**

# Conclusions

- We successfully simulated 3D tri-axial induction measurements by combining the use of a Fourier series expansion in a non-orthogonal system of coordinates with a 2D high-order, self-adaptive *hp* finite-element method.
- Dip angle effects on tri-axial tools are larger than on more traditional induction logging instruments.
- Anisotropy effects on $H_{xx}$ and $H_{yy}$ decrease with increasing dip angle, while those on $H_{zz}$ increase.
- $H_{xx}$ at 20 kHz exhibits smaller variations than at 2 MHz.
- Differences in stability between conductive and resistive mandrels in the presence of tool eccentricity.

# Acknowledgements

**Sponsors of UT Austin's consortium on Formation Evaluation:**

Anadarko Petroleum Corporation
ارامكو السعودية Saudi Aramco
Baker Hughes
Baker Atlas
bhpbilliton
bp
Chevron
ConocoPhillips
Agip
Eni
ExxonMobil
HALLIBURTON
IMP Innovar INSTITUTO MEXICANO DEL PETRÓLEO
Marathon Oil Corporation
BR PETROBRAS
Schlumberger
Shell
StatoilHydro
TOTAL
Weatherford